Photoselection in polarized photolysis experiments on heme proteins

Anjum Ansari, Colleen M. Jones, Eric R. Henry, James Hofrichter, and William A. Eaton
Laboratory of Chemical Physics, Building 2, National Institute of Diabetes and Digestive and Kidney Diseases, National Institutes of Health, Bethesda, Maryland 20892 USA

ABSTRACT Polarized photolysis experiments have been performed on the carbon monoxide complex of myoglobin to assess the effects of photoselection on the kinetics of ligand rebinding and to investigate the reorientational dynamics of the heme plane. The results are analyzed in terms of the optical theory developed in the preceding paper by Ansari and Szabo. Changes in optical density arising from rotational diffusion of the photoselected population produce large deviations from the true geminate ligand rebinding curves if measurements are made with only a single polarization. The apparent ligand rebinding curves are significantly distorted even at photolysis levels greater than 90%. These deviations are eliminated by obtaining isotropically-averaged optical densities from measurements using both parallel and perpendicular polarizations of the probe pulse. These experiments also yield the optical anisotropy, which gives a novel method for accurately determining the degree of photolysis, as well as important information on the reorientational dynamics of the heme plane. The correlation time for the overall rotational diffusion of the molecule is obtained from the decay of the anisotropy. The anisotropy prior to rotational diffusion is lower than that predicted for a rigidly attached, perfectly circular absorber, corresponding to an apparent order parameter of $S = 0.95 \pm 0.02$. Polarized absorption data on single crystals suggest that the decreased anisotropy results more from internal motions of the heme plane which take place on time scales shorter than the duration of the laser pulse (10 ns) than from out-of-plane polarized transitions.

INTRODUCTION

Photodissociation experiments play an increasingly important role in the investigation of the kinetics and dynamics of ligand binding and conformational changes in heme proteins (1–16). In the most frequently performed experiment a linearly polarized laser pulse is used to photodissociate the heme-bound ligand, and a second linearly polarized pulse is used to probe the molecule at a variable time-delay after excitation. In most experiments photolysis is incomplete. This may occur simply because it is not possible to obtain sufficient laser energy to photodissociate all molecules in the sample, or it may be carried out by design. Partial photolysis experiments are particularly useful in investigating hemoglobin kinetics. Systematic changes in photolysis are used to create variable distributions of ligation states of the tetramer, making it possible to distinguish between tertiary and quaternary conformational changes (3, 8, 17–19). An important consequence of incomplete photodissociation is the creation of an anisotropic distribution of molecular species by photoselection (20). Photoselection is the preferential photodissociation (i.e., "selection") of molecules oriented with their transition moments parallel to the electric vector of the excitation pulse. Although, as we shall see in this work, the influence of photoselection on the measurement of ligand rebinding kinetics is quite substantial, its effect has largely been ignored.

In order to obtain accurate kinetic progress curves for geminate rebinding of oxygen and carbon monoxide on the picosecond to microsecond time scale, it is essential to understand the consequences of photoselection. A qualitative picture of these effects is shown schematically in Fig. 1. It is known from polarized absorption studies on single crystals that, to a good approximation, hemes behave like circularly-symmetric absorbers of linearly polarized light at the wavelengths used in photolysis experiments (21). Circular absorbers have the property that there is equal absorption of light polarized parallel to any direction in the plane defined by the circle, and no absorption of light polarized perpendicular to the plane.[1] The probability of photodissociation is therefore greater when the porphyrin planes of heme-ligand complexes are oriented parallel to the electric vector of a linearly polarized excitation pulse, than when they are oriented perpendicular. Immediately after photodissociation, the sample exhibits linear dichroism because the distribution of each species is no longer isotropic. If the sample is probed with light linearly polarized parallel (perpendicular) to the excitation polarization, the fraction of unliganded hemes will appear to be greater (less) than the true value (Fig. 1). As the molecular orientations randomize by rotational diffusion, the linear dichroism decays (Fig. 1). This decay contributes an apparent increase in the fraction of liganded hemes for measurements with the parallel orientation of the probe polarization. For the perpendicular orientation the apparent fraction of liganded hemes decreases. Thus, rotational diffusion interferes with an accurate measurement of the kinetics of ligand binding taking place on the same time scale.

The effect of photoselection can be eliminated in two ways.[2] One is to orient the polarization of the probe light

[1] Circularly-symmetric absorbers of linearly polarized light, or simply circular absorbers, are often called planar absorbers. The property of circular absorption requires that either the ground state or the excited state (but not both) be two-fold degenerate. Non-degenerate transitions exhibit linear absorption, while three-fold degenerate transitions exhibit spherically symmetric absorption.

[2] Photoselection also affects the distribution of ligation states in hemoglobin (18). If the probability of absorbing a photon by each heme of the tetramer were uncorrelated, the distribution of liganded hemes in the tetramer would be binomial. However, since the four hemes of hemoglobin are roughly parallel (21), excitation with linearly polar-

0006-3495/93/03/852/17 $2.00

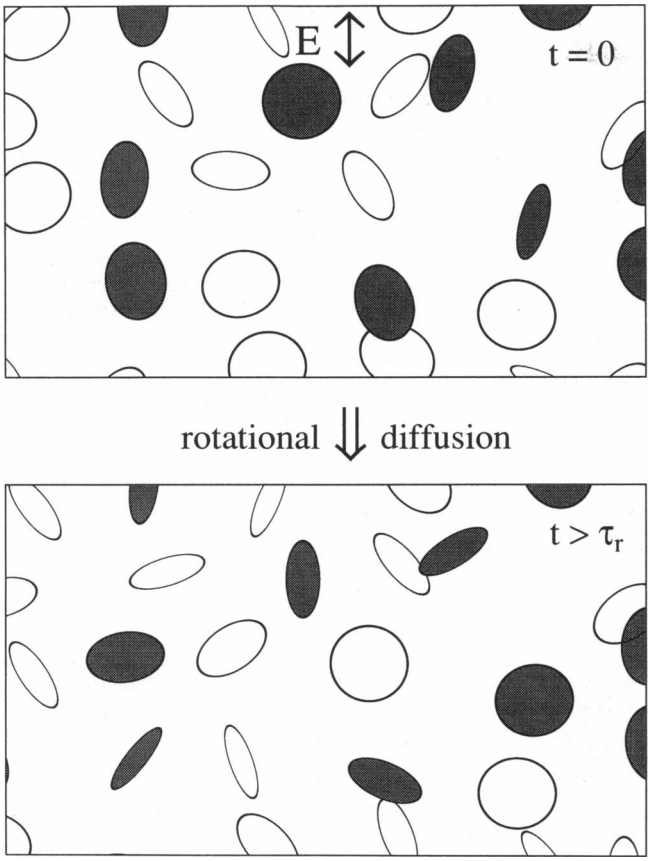

FIGURE 1 Schematic diagram showing the influence of photoselection on the measurement of the fraction of liganded hemes. The molecules are represented as circular discs to indicate circular absorption. Shaded discs correspond to photodissociated molecules. See text for description.

at the so-called "magic angle" of 54.7° relative to the excitation polarization. Since $\cos^2 54.7° = 1/3$, measurements at this angle result in a two-fold weighting of the perpendicular optical density compared to the parallel optical density, and are therefore equivalent to measuring the isotropically averaged optical density. This method is useful for optically thin samples or at low degrees of photolysis, where the linear dichroism is small. At intermediate degrees of photolysis, where the linear dichroism is largest, the polarization direction is rotated by the sample toward the more weakly absorbing direction. In this case the isotropically averaged optical density is no longer measured (22).

A more useful way of eliminating photoselection effects is to measure optical densities in both polarizations, and to obtain the isotropically-averaged value at each wavelength from the relation:

$$\Delta OD_{iso} = \tfrac{1}{3}(\Delta OD_{\parallel} + 2\Delta OD_{\perp}), \quad (1)$$

where ΔOD is the difference in optical density between the photodissociated and unphotodissociated samples. There are several advantages to this approach. First, accurate isotropically averaged optical density changes are obtained at all degrees of photolysis. Second, there is important dynamical information in the absorption anisotropy obtained from the data in both polarizations. The absorption anisotropy $r(x, t, \lambda_p)$ is a function of the degree of photolysis (x), time (t), and probe wavelength (λ_p), and is defined as:

$$r(x, t, \lambda_p) = \frac{\Delta OD_{\parallel} - \Delta OD_{\perp}}{\Delta OD_{\parallel} + 2\Delta OD_{\perp}}. \quad (2)$$

Its magnitude and decay rate provide important information on the heme and protein dynamics. For example, the anisotropy of the carbon monoxide infrared absorption bands following partial photolysis have been used to investigate the geometry and dynamics of carbon monoxide bound to the heme of hemoglobin and myoglobin. Both picosecond time-resolved experiments at room temperature (23–25) and steady state experiments at low temperature have been performed (26). Finally, the magnitude of the absorption anisotropy gives an independent and sensitive measure of the degree of photolysis.

In the preceding paper by Ansari and Szabo (27), theoretical relations for optical density changes measured with polarized light and for the absorption anisotropy as a function of time and laser intensity are derived. Expressions are developed for short excitation pulses and for finite pulses of sufficient width to allow both heme reorientation and kinetics during excitation. The theory includes the effects of deviations from perfectly circular absorption by the heme as well as the various types of reorientational motion of the heme plane: internal motion from equilibrium fluctuations, overall motion of the entire protein, and reorientation associated with conformational changes.

In this paper we compare the theoretical results with experimental results using 10 ns laser pulses on myoglobin in glycerol/water solvents at ambient temperatures. As predicted by the theory, we find that changes in the observed optical densities resulting from rotational diffusion of the photoselected population produce large deviations from the true ligand binding curves for myoglobin in a glycerol/water solvent. These effects are significant even at photolysis levels greater than 90%. The dependence of the experimental absorption anisotropies on the degree of photolysis agrees with the theoretical dependence, but the experimental values prior to rotational diffusion are ~0.9 times the values predicted for a rigidly attached, circular absorber. Three possible contributions to lowering the anisotropy are discussed: deviations from perfectly circular absorption due to an underlying out-of-plane polarized transition, fluctuations in

ized light introduces deviations from this binomial distribution. These effects are not eliminated by working at the magic angle or taking the isotropic average and have to be considered in order to accurately monitor the kinetics of the various ligation states of the tetramer.

the orientation of the heme plane, and a change in the average orientation of the heme plane resulting from a conformational change of the globin in response to ligand dissociation. In the following paper by Henry (28) a theoretical estimate of the contribution from fluctuations in the heme plane is obtained from molecular dynamics simulations.

METHODS

Sample preparation

Sperm whale skeletal muscle metmyoglobin was purified as described previously (29) and stored in liquid nitrogen. Measurements were made in either 50 or 75% glycerol-water solutions buffered at pH 7.0 with 0.1 M potassium phosphate. The 50% glycerol-water (56% wt/wt) solution was prepared by mixing equal volumes of glycerol and aqueous protein solution, while the 75% glycerol-water (79% wt/wt) solution was prepared by mixing 3 volumes of glycerol with one volume of aqueous protein solution. The carbon monoxide (CO) complex was formed by equilibrating the solution with one atmosphere of CO and reducing the heme anaerobically with sodium dithionite before loading into a cuvette (Wilmad WG-814 EPR cell).

Transient spectrometer

Time resolved absorption spectra were measured with a laser spectrometer that is described in detail elsewhere (18, 19, 30, 31). The second harmonic of a Nd:YAG laser pulse (10 ns fwhm at 532 nm) was used to photolyze the carbon monoxide complex; the third harmonic of another Nd:YAG laser pulse (10 ns fwhm at 355 nm) was used to excite the fluorescence of a dye, stilbene 420 in methanol, to provide a pulsed broad band (385–480 nm) probe source. The time delays between the excitation and the probe pulses were controlled electronically, and were logarithmically spaced with 12–15 time points per decade. The transmitted intensities of the probe beam were recorded on a silicon vidicon detector read by an OMA detector controller. The measured spectra were photolyzed minus unphotolyzed optical densities, averaged over 45–50 laser shots for each time delay. Difference spectra as a function of time were recorded for varying excitation intensities, thereby varying the fraction of hemes photolyzed. The excitation intensity was varied by inserting neutral density filters into the beam path. For each level of photolysis, measurements were taken with the polarization of the excitation beam oriented both parallel and perpendicular to the probe beam. The probe beam was polarized with sheet polaroid (extinction ratio 0.005); the more intense excitation beam was polarized using an air-gap Glan-Thompson prism with an extinction ratio of $<5 \times 10^{-5}$. A $\lambda/2$ waveplate positioned between the polarizing prism and the sample was used to rotate the polarization of the excitation beam.

Singular value decomposition of data

Each data set consisted of difference spectra at time intervals from about -10 ns to $+10$ μs in the 50% glycerol-water sample and from -10 ns to +90 ms in the 75% glycerol-water sample. Each set of difference spectra was first analyzed using singular value decomposition (SVD), which transforms a data matrix $\mathbf{D}$ into a product of three matrices, $\mathbf{D} = \mathbf{USV}^{\mathrm{T}}$ (8, 32, 33). The columns of $\mathbf{U}$ are a set of orthonormal basis spectra that describe all of the spectra in the data matrix $\mathbf{D}$; the corresponding columns of $\mathbf{V}$ are the amplitudes of the spectral components as a function of time; and $\mathbf{S}$ is a diagonal matrix with non-negative elements (singular values), which are a measure of the contribution of the corresponding basis spectrum to the data matrix. SVD has the useful property that the components with the k largest singular values provide the best (in the least squares sense) k-component fit to all the data.

In order to compare the data measured under different conditions (i.e., two polarizations at varying degrees of photolysis), a 'global' data matrix was constructed from the first 12 components of the individual experiments. Data from different experiments were interpolated onto a common time axis (18, 19). The SVD of this matrix provides a convenient and compact representation of all of the data with a common set of basis spectra. The largest contribution to noise in these measurements was baseline offsets resulting from intensity fluctuations of the probe laser. These offsets were uncorrelated with delay time, and were removed as described by Jones et al. (19). Small differences in the degree of photolysis between a pair of parallel and perpendicular polarization experiments arose from drifts in laser intensity and from differential reflection losses for the two polarizations. The amplitudes of the difference spectra at times much longer than the rotational correlation time of the molecule were used to correct for these differences, since these amplitudes are proportional to the degree of photolysis. The spectra corresponding to the parallel and perpendicular data sets were linearly interpolated to photolysis levels intermediate to the photolysis levels of the individual data sets.

Probing with finite pulses

In the preceding paper Ansari and Szabo (27) calculated the optical density change and absorption anisotropy that would be observed with infinitely sharp (δ-function) probe pulses. In this paper we extend the theoretical framework to include finite probe pulses. We show that the deviations from the δ-function probe limit are maximal when the excitation and probe pulses overlap (29), and are negligible at times that are long compared to the duration of the probe pulse. The observed optical density change at any time t (where t is defined as the difference between the peaks of the excitation and the probe pulses) is derived from transmitted intensities that are averaged over the temporal profile of the probe pulse.

We define $I_p(\tau)$ to be the normalized probe pulse profile, centered at $\tau = 0$, which is incident upon the sample ($\int I_p(\tau)\,d\tau = 1$). We define ϵ_A^0 and ϵ_B^0 as the isotropic extinction coefficients for MbCO and Mb, respectively, at the probe wavelength λ_p. The integrated probe light intensity which reaches the detector prior to photolysis, I_r, is:

$$I_r = \int_{-\infty}^{+\infty} I_p(\tau)\, 10^{-\epsilon_A^0 cl}\, d\tau = 10^{-\epsilon_A^0 cl}, \qquad (3)$$

where c is the concentration of the sample, and l is the sample path length. The probe light intensity at the detector after excitation depends upon the relative populations of the two spectrally distinct states and their orientational distributions. In the preceding paper we defined $f(t)$ as the normalized change in absorbance of the sample after excitation. The absolute absorbance of the sample after excitation is therefore $cl[(\epsilon_B^0 - \epsilon_A^0)f(t) + \epsilon_A^0]$, where $cl(\epsilon_B^0 - \epsilon_A^0)$ is the maximum change in absorbance when all the MbCO molecules are photolyzed. The experimentally measured signal, $I_s(t)$, is the integrated light intensity of a finite probe pulse at the detector at time t after excitation; it is obtained by convoluting the transmittance of the sample with the probe pulse profile:

$$I_s(t) = \int_{-\infty}^{+\infty} I_p(t-\tau)\, 10^{-cl[(\epsilon_B^0 - \epsilon_A^0)f(\tau) + \epsilon_A^0]}\, d\tau \qquad (4)$$

The experimentally observed change in absorbance, $f_{\mathrm{exp}}(t)$, becomes:

$$f_{\mathrm{exp}}(t) = \frac{-1}{cl(\epsilon_B^0 - \epsilon_A^0)} \log_{10} \frac{I_s(t)}{I_r} = \frac{-1}{cl(\epsilon_B^0 - \epsilon_A^0)} \times \log_{10}\left(\int_{-\infty}^{+\infty} I_p(t-\tau)\, 10^{-cl[(\epsilon_B^0 - \epsilon_A^0)f(\tau)]}\, d\tau \right), \qquad (5)$$

where we have normalized the change in absorbance with $cl(\epsilon_B^0 - \epsilon_A^0)$. One may readily verify that when the probe pulse is a δ-function,

$I_p(\tau) = \delta(\tau)$, or when $f(t)$ is approximately a constant over the duration of the probe pulse, then $f_{exp}(t) \approx f(t)$. In the limit of thin samples (low optical densities) or at the wavelength where the difference between the extinction coefficients of MbCO and Mb is small, i.e., $\epsilon_A^0 \approx \epsilon_B^0$, Eq. 5 simplifies to:

$$f_{exp}(t) = \int_{-\infty}^{+\infty} I_p(t - \tau) f(\tau)\, d\tau. \qquad (6)$$

Thus, in the thin sample limit, the change in optical density observed with finite pulses is obtained by convoluting the change in optical density calculated for δ-function probe pulses with the shape of the finite pulse.

The effect of convoluting with finite probe pulses is illustrated in Fig. 2, which represents simulations of the change in optical density observed as a function of the time delay between the excitation and probe pulses. Both pulses have been represented as gaussian pulses with about 10 ns (fwhm) pulse-widths. $t = 0$ is defined as the time when the two pulses coincide; negative times indicate that the peak of the probe pulse is earlier in time than the peak of the excitation pulse. Because the widths of the two pulses are finite, the observed change in optical density is non-zero at these negative times. We consider the reaction scheme (29):

$$A \underset{k_1}{\overset{h\nu}{\rightleftarrows}} B \underset{k_3}{\overset{k_2}{\rightleftarrows}} C, \qquad (7)$$

where A corresponds to MbCO, B to Mb with the photodissociated CO still inside the protein, and C to Mb with CO in the solvent. In Fig. 2, we compare $f(t)$, simulated using the theory of excitation with finite pulses described in section 5 of the preceding paper, with $f_{exp}(t)$, obtained by convoluting $f(t)$ with the probe pulse profile (Eq. 6). The deviations between $f(t)$ and $f_{exp}(t)$ are maximal at times that are short compared to the duration of the probe pulse. At times longer than ~10 ns, the deviations are negligible. The simulations also show that the time at which $f_{exp}(t)$ reaches a maximum is, in all cases, later than when the two pulses coincide and depends in detail upon the rate parameters in Eq. 7 and the excitation intensity. Fig. 2 *a* illustrates the effect of varying the ligand rebinding amplitude: as the rebinding amplitude increases, the maximum in the optical density changes appears earlier. Fig. 2 *b* illustrates the effect of varying the excitation intensity. The time at which the optical density reaches a maximum decreases with increasing intensity.

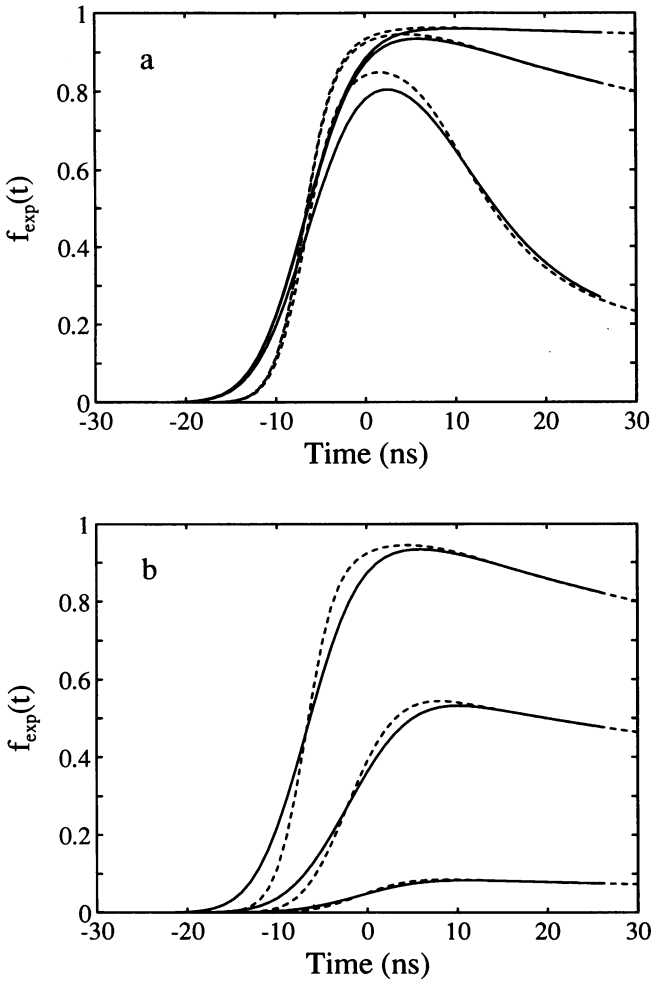

FIGURE 2 Simulation of photodissociation and detection with finite excitation and probe pulses. The dashed curves are the normalized change in absorbance $f(t)$ measured with a δ-function probe pulse after excitation with a gaussian pulse (fwhm = 10 ns) plotted as a function of time; the continuous curves are the normalized change in absorbance $f_{exp}(t)$ that would be observed when the system is probed with another gaussian pulse (fwhm = 10 ns) and are obtained by convoluting $f(t)$ with the probe pulse profile (Eq. 6). $f(t)$ is obtained for the reaction scheme in Eq. 7 using the theory of excitation with finite pulses described in the preceding paper; from Eq. 3.45 of the preceding paper and at the magic angle $[P_2(\hat{\mathbf{e}} \cdot \hat{\mathbf{p}}) = 0]$ we obtain $f(t) = 1 - a_0(\lambda_e, t)$; $a_0(\lambda_e, t)$ is calculated for the reaction scheme (Eq. 7) by solving the coupled differential equations (Eq. 5.4) of the preceding paper for the coefficients a_1, b_1, c_1, subject to the initial conditions $a_1 = \delta_{10}$, $b_1 = 0$, $c_1 = 0$, that correspond to the system being in the liganded state A prior to photodissociation. (*a*) The normalized change in absorbance calculated for varying values of the geminate rebinding amplitude by varying the ligand rebinding rate k_1 in Eq. 7. $k_2 = 10^7\ s^{-1}$ and $k_3 = 0$ for all the simulations. Upper curves: $k_1 = 10^6\ s^{-1}$; middle curves: $k_1 = 10^7\ s^{-1}$; lower curves: $k_1 = 10^8\ s^{-1}$. The intensity of the excitation pulse is the same in all three cases and there is no rotational diffusion within the pulse. (*b*) The normalized change in optical density calculated for varying values of the excitation intensity, with $k_1 = 10^7\ s^{-1}$, $k_2 = 10^7\ s^{-1}$, $k_3 = 0$.

RESULTS AND DISCUSSION

In order to demonstrate the influence of photoselection on absorption measurements following partial photolysis of the carbon monoxide complex of myoglobin (MbCO), we performed two series of experiments in 50 and 75% glycerol-water. Under these conditions the rotational correlation time of the molecule is long compared to the duration of the excitation pulse (fwhm = 10 ns). In the first series of experiments Mb-minus-MbCO difference spectra in 50% glycerol-water were measured as a function of excitation laser intensity at a fixed time delay of 10 μs between the excitation and probe pulses. At times which are long compared to the rotational correlation time of the molecule, the amplitude of the difference spectrum is proportional to the fraction of hemes photolyzed and is independent of the polarizations of the excitation and probe pulses. The dependence of the fraction of hemes photolyzed on the excitation intensity depends upon the properties of the absorber (34). In the absence of any photoselection effects this fraction approaches saturation exponentially. These experiments demonstrate the deviations from an exponen-

tial approach to saturation due to photoselection effects. In order to accurately determine the fraction of heme-CO complexes that are photodissociated by extrapolating the observed amplitudes of the difference spectra to infinite excitation intensity, the effects of photoselection have to be included in the theoretical description.

In the second series of experiments, difference spectra at varying degrees of photolysis were measured in both 50 and 75% glycerol-water solutions at time delays ranging from overlap of excitation and probe pulses to time delays which are long compared to the rotational correlation time of the molecule. Spectra were measured with the orientation of the electric vector of the linearly-polarized excitation beam both parallel and perpendicular to that of the probe beam. These experiments demonstrate the effects of photoselection and rotational diffusion on the measurement of ligand rebinding kinetics. In addition, a comparison of the experimentally observed absorption anisotropies with the theoretically predicted values provides an independent and more accurate measure of the degree of photolysis. We find that the observed anisotropies are ~0.9 times that predicted for a perfectly circular, rigid absorber, and discuss the possible causes for this reduction.

Fractional photolysis versus excitation laser intensity

The orientational distribution of MbCO molecules that can rotationally diffuse or absorb a photon and dissociate is described by Eq. 2.2 of the preceding paper. If the rotational correlation time (τ_r) of the MbCO molecule is short compared to the excitation pulse-width, then all the molecules have equal probability of absorbing a photon and there is no photoselection. The orientational distribution of MbCO molecules, $p_A(\Omega)$, at the end of the pulse is then given by

$$p_A(\Omega) = p_{eq}(\Omega)\exp(-\langle\epsilon_A(e,\Omega)\rangle I_0) = p_{eq}(\Omega)\exp(-\epsilon_A^0(\lambda_e)I_0). \quad (8)$$

I_0 is proportional to the integrated intensity of the excitation pulse and is obtained by integrating $[\ln(10)n_e(t)\phi]/N_A$ over the pulse-width, where n_e is the number of incident photons per unit area per unit time, ϕ is the probability that CO will dissociate after the absorption of a photon, and N_A is Avogadro's number; Ω represents the angular coordinates that describe the orientation of the heme relative to the polarization directions of the excitation and probe pulses; $\epsilon_A(e,\Omega)$ is the extinction coefficient of the heme in the direction of the excitation polarization ($\hat{\mathbf{e}}$) and at the excitation wavelength λ_e, which, when averaged over the equilibrium distribution of molecules, yields the isotropic extinction coefficient $\epsilon_A^0(\lambda_e)$. Previous experiments on MbCO have shown that $\phi = 1$ (29), so that we can equate the fraction excited and the fraction photolyzed. The fraction of molecules that are photolyzed at the end of the pulse (x) is therefore:

$$x = 1 - \int p_A(\Omega)\,d\Omega = 1 - \exp(-\epsilon_A^0(\lambda_e)I_0), \quad (9)$$

and increases exponentially with increasing excitation intensity. If, on the other hand, the rotational correlation time of the molecule is long compared to the excitation pulse-width, the approach to saturation (i.e., 100% photolysis) is significantly slower. This is because the molecules that have their transition moments oriented perpendicular to the excitation polarization direction have a vanishingly small probability of absorbing a photon. The detailed dependence of the fraction photolyzed on the excitation intensity depends upon the absorption properties of the chromophore and its reorientational dynamics during excitation. In the preceding paper it is shown that, in the limit of slow reorientational dynamics of the chromophore, the fraction of molecules excited at the end of the pulse is given by:

$$x = 1 - \frac{1}{2}\int_0^{\pi} \exp(-\epsilon_A^0(\lambda_e)I_0[1 - \sigma P_2(\cos\theta)]) \times \sin\theta\,d\theta, \quad (10)$$

where P_2 is the second Legendre polynomial [$P_2(\cos\theta) = (1/2)(3\cos^2\theta - 1)$] and σ specifies whether the absorber is circular or linear. For a linear absorber ($\sigma = -2$), the fraction of molecules that are excited is given by:

$$x = 1 - \frac{1}{2}\int_0^{\pi} \exp(-3\epsilon_A^0(\lambda_e)I_0\cos^2\theta)\sin\theta\,d\theta \quad (11)$$

and, for a circular absorber ($\sigma = 1$), by:

$$x = 1 - \frac{1}{2}\int_0^{\pi} \exp\left(-\frac{3}{2}\epsilon_A^0(\lambda_e)I_0\sin^2\theta\right)\sin\theta\,d\theta. \quad (12)$$

Fig. 3 *a* compares the fraction of molecules that are excited in an ensemble of rapidly rotating molecules (no photoselection, Eq. 9) with the fraction excited when the rotational diffusion of the molecules is slow and the absorber is linear or circular (Eqs. 11–12); the molecules are assumed to be randomly oriented at equilibrium. The slowest approach to saturation is in the case of a linear absorber.

Experimentally, the fraction of photodissociated molecules is determined from the change in optical density immediately after excitation. In the preceding paper it is shown that for a two-state system, (the ligand-bound state A and the photodissociated state B), in which the hemes in both states have the same reorientational dynamics, the normalized change in optical density following a short intense pulse is given by:

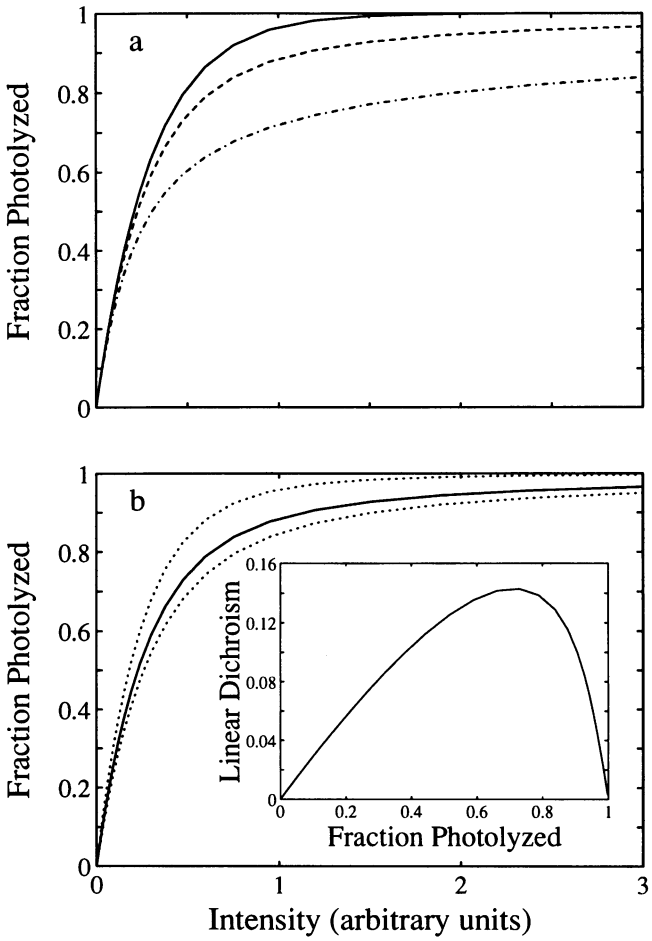

FIGURE 3 Simulation of the role of photoselection in determining the fraction of excited molecules. (*a*) The fraction of molecules that are excited with a δ-function excitation pulse is plotted as a function of the excitation intensity for isotropic (——) (Eq. 9), linear (– · – · –) (Eq. 11), and circular (---) (Eq. 12) absorbers. (*b*) The normalized change in optical density at $t = 0^+$ following excitation of a circular absorber with a δ-function excitation pulse, $f(0^+)$, calculated using Eq. 16, (with $a_0 (= 1 - x)$ and a_2 given by Eqs. 12 and 15, respectively), is plotted as a function of the excitation intensity. Upper curve: excitation and probe pulse polarizations are parallel ($\hat{\mathbf{e}} \cdot \hat{\mathbf{p}} = 1$); lower curve: excitation and probe pulse polarizations are perpendicular ($\hat{\mathbf{e}} \cdot \hat{\mathbf{p}} = 0$); middle curve: isotropic average obtained by setting $P_2(\hat{\mathbf{e}} \cdot \hat{\mathbf{p}}) = 0$ in Eq. 16. The linear dichroism $[(f_{\parallel}(0^+) - f_{\perp}(0^+) = 3a_2/10]$ is plotted in the inset as a function of the isotropic amplitude which is equal to the fraction photolyzed.

$$f(t, \lambda_p) = [1 - \Phi(t)]\Big[1 - a_0 + \frac{a_2}{5} P_2(\hat{\mathbf{e}} \cdot \hat{\mathbf{p}}) \frac{1}{\epsilon^0_B(\lambda_p) - \epsilon^0_A(\lambda_p)} \times (\epsilon^0_B(\lambda_p)\sigma_B(\lambda_p)\langle P_2(\hat{\mathbf{n}}_B(t) \cdot \hat{\mathbf{n}}_A(0))\rangle - \epsilon^0_A(\lambda_p)\sigma_A(\lambda_p)\langle P_2(\hat{\mathbf{n}}_A(t) \cdot \hat{\mathbf{n}}_A(0))\rangle)\Big] \quad (13)$$

where $1 - a_0$ is the fraction of molecules that are photodissociated and is given by Eq. 3.17 of the previous paper, and a_2 is proportional to the linear dichroism introduced in the sample by photoselection and is given by Eq. 3.18 of the preceding paper. For a circular absorber $\sigma = 1$, and, for a uniaxially symmetric absorber with a non-zero out-of-plane component, σ is given by Eqs. 3.5 and 3.8 of the preceding paper. $\hat{\mathbf{n}}_I$ is the normal to the heme plane in the state $I = A, B$ and $\Phi(t)$ is the probability that a photodissociated molecule rebinds a ligand at time t. The quantities in angled brackets in Eq. 13 denote reorientational correlation functions for the heme plane. The utility and power of the correlation function is that it contains all of the information on the reorientational dynamics of the heme, including equilibrium fluctuations, conformational relaxation, and overall motion of the protein due to rotational diffusion.

If the heme is approximated as a circular absorber ($\sigma = 1$) that has the same orientation in the two states ($\hat{\mathbf{n}}_A = \hat{\mathbf{n}}_B = \hat{\mathbf{n}}$), $f(t, \lambda_p)$ is independent of the probe wavelength and Eq. 13 simplifies to:

$$f(t) = \Big(1 - a_0 + \frac{a_2}{5} P_2(\hat{\mathbf{e}} \cdot \hat{\mathbf{p}})\langle P_2(\hat{\mathbf{n}}(t) \cdot \hat{\mathbf{n}}(0))\rangle\Big) \times [1 - \Phi(t)], \quad (14)$$

where $a_0 (= 1 - x)$ is given by Eq. 12 and a_2 is given by:

$$a_2 = \frac{5}{2}\int_0^{\pi} \exp\Big(-\frac{3}{2}\epsilon^0_A(\lambda_e) I_0 (1 - \cos^2\theta)\Big) \times P_2(\cos\theta) \sin\theta \, d\theta. \quad (15)$$

The normalized change in optical density immediately after the excitation pulse becomes:

$$f(0^+) = 1 - a_0 + \frac{a_2}{5} P_2(\hat{\mathbf{e}} \cdot \hat{\mathbf{p}}). \quad (16)$$

We will call $f(0^+)$ the apparent fraction photolyzed; it depends upon the relative orientation of the excitation and probe polarization directions. Fig. 3 *b* compares the real and apparent fraction of excited molecules for a circular absorber when the excitation and probe beams are parallel ($\hat{\mathbf{e}} \cdot \hat{\mathbf{p}} = 1$) or perpendicular ($\hat{\mathbf{e}} \cdot \hat{\mathbf{p}} = 0$) and the rotational correlation time of the molecule is long compared to the excitation pulse-width. For parallel polarizations the apparent fraction of photodissociated molecules is larger at all degrees of photolysis and saturates more rapidly than the real fraction, while for perpendicular polarizations the apparent fraction is smaller and saturates more slowly.

The normalized optical density change when the photoselected population has randomized, is given by:

$$f(t \gg \tau_r) = (1 - a_0)[1 - \Phi(t)], \quad (17)$$

where τ_r is the rotational correlation time of the molecule and $f(t \gg \tau_r)$ provides a measure of the real fraction of excited molecules, $x (= 1 - a_0)$. The fraction of hemes photolyzed in MbCO was measured by collecting a series of difference spectra at a fixed time delay ($t = 10$ μs) between the excitation and probe pulses after excitation with pulses of varying intensity. The conditions were se-

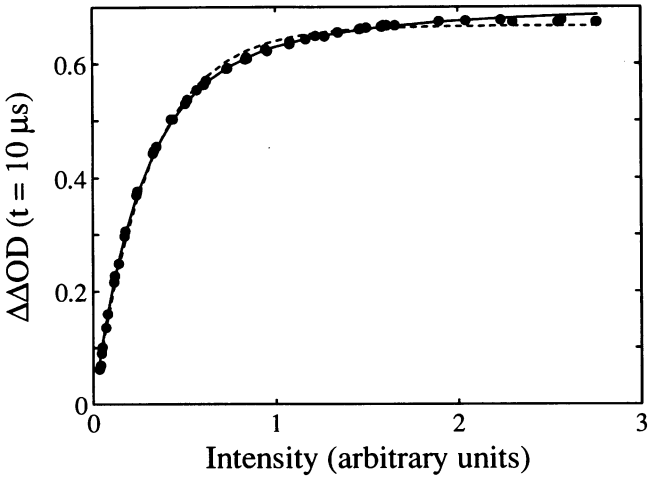

FIGURE 4 Intensity dependence of the fraction photolyzed. The amplitude of the difference spectrum, $\Delta\Delta OD$ (t = 10 μs), defined as ΔOD (438 nm, 10 μs) − ΔOD (422 nm, 10 μs), is obtained from the first SVD component of the measurements of the difference spectra at 10 μs and is plotted versus the excitation intensity. The fraction of hemes photolyzed is proportional to the spectral amplitude. The continuous curve is a fit to the data using Eq. 18 where a_0 (= 1 − x) is calculated for a circular absorber using Eq. 12; (1 − Φ)$\Delta\Delta OD_{max}$ in Eq. 18 is a fitting parameter with a best-fit value of 0.714 ± 0.02. The dashed curve is a fit to the data where a_0 (= 1 − x) is calculated for an isotropic absorber (no photoselection) using Eq. 9.

lected so that the rotational correlation time of the molecule τ_r (=200 ns in 50% glycerol-water at 5°C) was long compared to the duration of the excitation pulse and Eq. 17 could be used to compare experiment with theory. The amplitudes of the difference spectrum, $\Delta\Delta OD$ (t = 10 μs), that best fits the spectra for all excitation intensities (obtained from a singular value decomposition of all the spectra) are plotted in Fig. 4 as a function of the excitation intensity. The dependence of the observed amplitudes on the excitation intensity may be written as:

$$\Delta\Delta OD\,(I_0, t = 10\ \mu s) = f(I_0, t = 10\ \mu s)\Delta\Delta OD_{max} = (1 - a_0(I_0))[1 - \Phi\,(t = 10\ \mu s)]\Delta\Delta OD_{max}, \quad (18)$$

where we have substituted for $f(t)$ from Eq. 17. $\Delta\Delta OD_{max}$ is the maximum amplitude of the difference spectrum when all the molecules are photodissociated. The experimental data were fit to the theory for a circular absorber in the limit of slow rotational diffusion, using Eqs. 12 and 18 ($x = 1 - a_0$). In carrying out the fit the product of $\Delta\Delta OD_{max}$ and [1 − Φ (t = 10 μs)] and a scale factor which relates the experimental excitation intensities to absolute intensities were used as fitting parameters. The fit to the experimental data, shown in Fig. 4, is excellent. A fit using an exponential curve (Eq. 9), on the other hand, shows systematic differences between the data and the fit and demonstrates qualitatively the effects of photoselection. The extrapolated value of the amplitude of the difference spectrum at infinite excitation intensity, $\Delta\Delta OD_{max}[1 - \Phi\ (t = 10\ \mu s)]$, obtained from a fit to the saturation curve, is 0.71 ± 0.02, indicating that the maximum photolysis level in this set of experiments is about 95 ± 3%. The determination of the degree of photolysis by this procedure requires an extrapolation to infinite laser intensity. A more accurate method, which is based on extrapolating the measured anisotropies to zero, is discussed below.

Kinetics of ligand rebinding

In this set of experiments time-resolved spectra were measured at various time delays following photodissociation with both parallel and perpendicular polarizations of the probe pulse. Fig. 5 shows the spectral surfaces measured in 75% glycerol-water at 20°C at ~80% photolysis. At short times the two spectral surfaces differ by an amount that is equal to the linear dichroism induced in the sample by photoselection (Fig. 5 *c*). The linear dichroism decays both because the photodissociated ligand rebinds and because the photoselected population reorients to a random distribution through rotational diffusion. A total of 14 such spectral surfaces were measured at varying degrees of photolysis in 75% glycerol-water at 20°C and 22 surfaces were measured in 50% glycerol-water at 5°C. The spectra measured under each set of conditions were analyzed using the SVD procedure. Fig. 6 shows the first four components of the singular value decomposition of the parallel polarization data in 75% glycerol-water. About 96% of all the data is described by the first component, which is the average Mb-minus-MbCO difference spectrum at all times and photolysis levels; the corresponding amplitudes provide a very good first approximation to the fraction of deoxyhemes. The higher order components, which represent deviations from the average spectrum, include spectral changes of the deoxy photoproduct (~3%), spectral distortions from inhomogeneous photolysis across the sample at intermediate levels of photolysis (~0.5%), and instrumental nonlinearities (<0.3%). The spectral changes of the deoxyheme photoproduct spectra are presumed to result from protein conformational changes, and the kinetics of these changes are discussed in detail elsewhere (16). In this paper we consider the effects of photoselection on the ligand rebinding kinetics and restrict most of the analysis to the first component.

We now consider in detail the effect of using linearly-polarized excitation and probe pulses on the ligand rebinding kinetics. When the polarization of the excitation and probe beams are parallel, $P_2(\hat{\mathbf{e}}\cdot\hat{\mathbf{p}}) = 1$, and the normalized change in optical density is, from Eq. 14:

$$f_{\parallel}(t) = \left(1 - a_0 + \frac{a_2}{5}\langle P_2(\hat{\mathbf{n}}(t)\cdot\hat{\mathbf{n}}(0))\rangle\right)[1 - \Phi(t)] \quad (19)$$

while for perpendicular orientations $P_2(\hat{e}\cdot\hat{p}) = -1/2$, and Eq. 14 becomes:

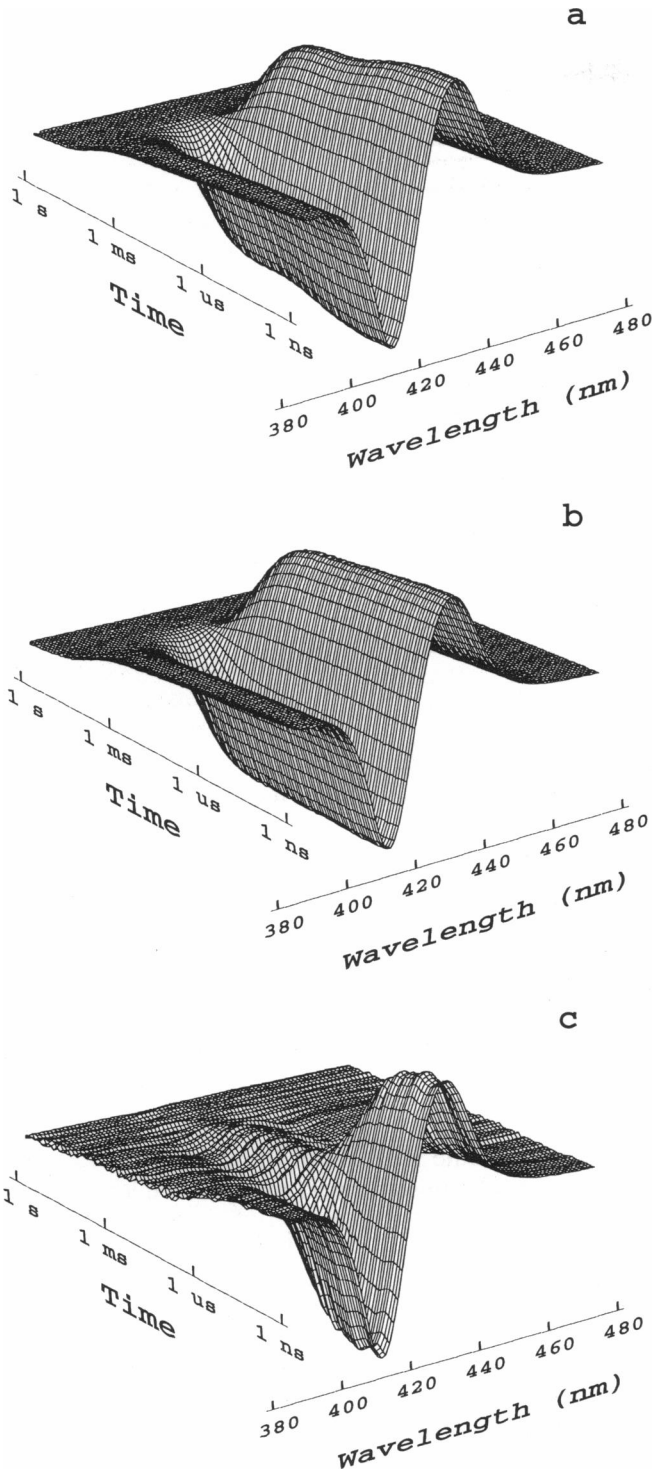

FIGURE 5 Difference spectra and linear dichroism decay following 80% photolysis of MbCO in 75% glycerol-water at 20°C. (*a*, *b*) Transient spectra measured as a function of time with the polarization of the probe pulse (*a*) parallel and (*b*) perpendicular to the polarization of the excitation pulse. The spectra shown were reconstructed from the first eleven components of the singular value decomposition of all the data after removal of the baseline offsets due to intensity fluctuations of the probe beam (19). (*c*) Linear dichroism decay (×10) calculated from the difference between the spectral surfaces in *a* and *b*.

$$f_{\perp}(t) = \left(1 - a_0 - \frac{a_2}{10}\langle P_2(\hat{\mathbf{n}}(t)\cdot\hat{\mathbf{n}}(0))\rangle\right)[1 - \Phi(t)]. \quad (20)$$

For measurements in a single polarization the ligand rebinding kinetics and reorientational dynamics are not separable; the change in the optical density is given by the product of two time-dependent terms, one which arises from the dynamics of heme reorientation and the other from ligand rebinding.

Experimentally we obtain $\Delta\Delta OD_{\parallel}(x,t)$ and $\Delta\Delta OD_{\perp}(x,t)$, the amplitude of the difference spectrum at each level of photolysis (x) in the parallel and perpendicular geometry, respectively, averaged over all wavelengths, from the first SVD component. $\Delta\Delta OD(x,t)$ is proportional to $f(t)$. The proportionality constant, $\Delta\Delta OD_{max}$ at 100% photolysis, is not known a priori. Fig. 7 shows the observed amplitudes in 75% glycerol-water at 20°C as a function of time and degree of photolysis. The earliest time shown is when the observed signal reaches a maximum and is assigned a value of 10 ns based on the simulations shown in Fig. 2. Note that the amplitude of the difference spectrum is independent of the polarization at times longer than ~3 μs, when the orientational distribution of the photoselected population is randomized.

The isotropically averaged optical density change calculated from Eq. 1 is also shown in Fig. 7. Only the isotropically averaged optical density changes accurately monitor the kinetics of ligand rebinding. The fraction of proteins that have not rebound a ligand at time t, $[1 - \Phi(t)]$ (the survival probability of the photodissociated CO), may be obtained by taking the ratio of the isotropic amplitude at time t with the isotropic amplitude measured immediately after excitation. In the case where the experiment is performed with the excitation beam polarized either parallel or perpendicular to the probe beam, the apparent survival probability is influenced by the reorientational dynamics of the heme plane. For measurements in the parallel configuration, the molecules that are photolyzed are preferentially probed, and the fraction of deoxy hemes appears to be larger than the true value (Fig. 1). Rotational diffusion decreases the fraction of photolyzed molecules that are probed, producing an apparent increase in the fraction of molecules that rebind a ligand (Fig. 1). In the perpendicular configuration, the opposite is the case. Initially molecules that are unphotolyzed are probed preferentially and the apparent fraction photolyzed is lower than the true value. In the absence of any ligand rebinding, rotational diffusion would produce an apparent ligand dissociation in the perpendicular configuration. In the presence of ligand rebinding the net result is an apparent decrease in the fraction of molecules that rebind a ligand.

The effects of photoselection and rotational diffusion on the apparent ligand rebinding amplitudes are shown in Fig. 8. At the lowest levels of photolysis the effects of

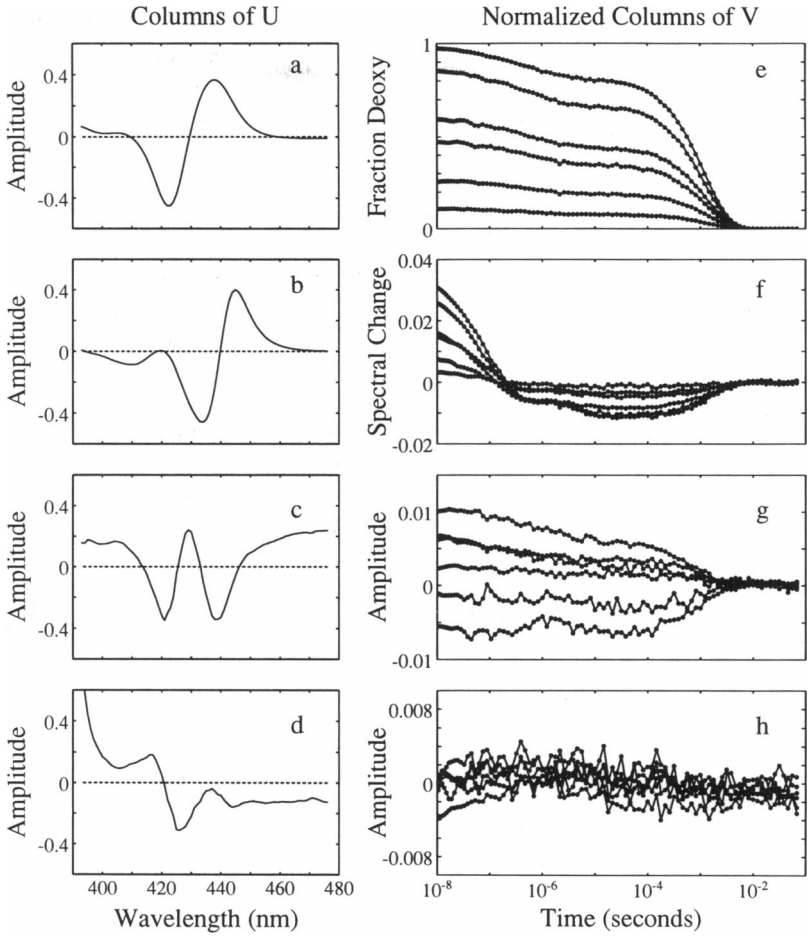

FIGURE 6 Singular value decomposition of the transient spectra in 75% glycerol-water at 20°C obtained with the parallel orientation of the excitation and probe pulses and for varying excitation intensities. (*a–d*): The first four spectral components (columns of U), after removal of the component corresponding to the baseline offsets (19), are shown. (*e–h*): The corresponding amplitudes of the spectral components (columns of V) are plotted as a function of time for various degrees of photolysis. The V components have been multiplied by the corresponding singular values and then normalized such that the first V component extrapolates to 1 for 100% photolysis at t = 10 ns.

photoselection are maximal. The apparent ligand rebinding amplitude is more than twice the true value in the parallel configuration, and only one-tenth the true value in the perpendicular configuration. At high levels of photolysis the apparent rebinding amplitudes approach the value observed in the isotropically averaged data. Note, however, that the effects are significant even at photolysis levels of ~95% (the maximum photolysis in our experiments). As expected, the isotropically averaged rebinding amplitudes, from which photoselection effects have been removed, are independent of the degree of photolysis.

Absorption anisotropy and heme reorientation dynamics

A major advantage of measuring spectra with both polarizations is that the decay of the absorption anisotropy obtained from such measurements yields useful and interesting information on the molecular dynamics of heme reorientation. In addition, the magnitude of the anisotropy obtained immediately after the pulse provides an accurate measure of the degree of photolysis. The absorption anisotropy, $r(x, t)$, at each level of photolysis (x) is obtained from:

$$r(x, t) = \frac{\Delta\Delta OD_{\parallel} - \Delta\Delta OD_{\perp}}{\Delta\Delta OD_{\parallel} + 2\Delta\Delta OD_{\perp}}, \qquad (21)$$

and represents an average anisotropy (averaged over all probe wavelengths). Fig. 9 shows the absorption anisotropy decay at various degrees of photolysis in 75% glycerol-water (20°C) and in 50% glycerol-water (5°C). The results show that the decay of the absorption anisotropy is independent of the degree of photolysis, and is characterized by a single relaxation. Since $\Delta\Delta OD$ is proportional to $f(t)$, the absorption anisotropy decay following a short intense pulse is obtained from Eqs. 19, 20 and 21:

$$r(x, t) = \frac{1}{10}\frac{a_2}{1 - a_0}\langle P_2(\hat{\mathbf{n}}(t)\cdot\hat{\mathbf{n}}(0))\rangle. \qquad (22)$$

In the limit of a short excitation pulse the anisotropy decay is independent of the details of the ligand rebind-

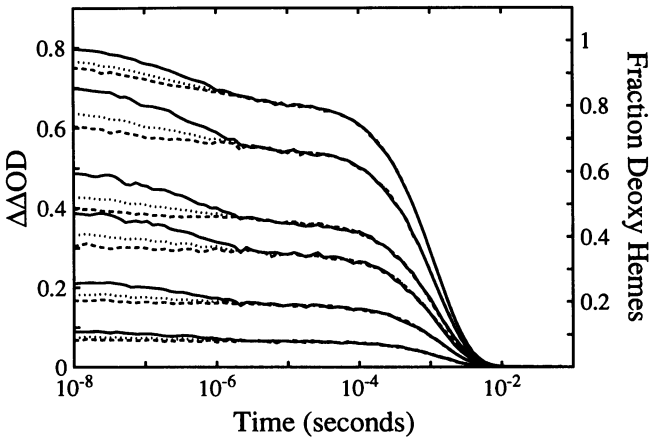

FIGURE 7 Amplitude of the transient spectra in 75% glycerol-water at 20°C. The amplitude of the difference spectrum, $\Delta\Delta OD$, defined as ΔOD(438 nm) − ΔOD(422 nm), is obtained from the first component of the singular value decomposition of the data (see Fig. 6 *e*) and plotted as a function of the time delay between the excitation and probe pulses, at various degrees of photolysis. Measurements were made with the polarization of the probe pulse parallel (continuous curve) and perpendicular (dashed curve) to the polarization of the excitation pulse. The dotted curves are the corresponding amplitudes for the isotropic data obtained using Eq. 1. The degrees of photolysis shown are 9, 22, 41, 52, 77, and 95%. The normalized amplitudes, indicated on the right, correspond to the fraction deoxy hemes in the case of the isotropic data; they are obtained by dividing the curves by $\Delta\Delta OD_{max} = 0.818$ (the maximum amplitude at 100% photolysis obtained from a fit to the anisotropy data in Fig. 10).

ing kinetics, and its decay is described by the reorientational correlation function. If we neglect any internal motions and assume that the heme is rigidly attached to the protein, the reorientational correlation function decays with a set of time constants which characterize the rotational diffusion of the entire molecule. For a spherical molecule there is a single rotational correlation time, τ_r, and the anisotropy decay is given by:

$$r(x, t) = \frac{1}{10}\frac{a_2}{1 - a_0}\exp(-t/\tau_r) \qquad (23)$$

The rotational correlation time $\tau_r = 1/6D_r$, where D_r is the rotational diffusion constant of the molecule.

In order to determine the rotational correlation time of myoglobin, the anisotropy decay curves were averaged over all degrees of photolysis. This average was obtained as the first component of the SVD of the individual anisotropy decay curves, after weighting the individual decay curves by the reciprocal of the noise in the curve. The fit of the average anisotropy decay in 50% glycerol-water (5°C) to an exponentially decaying function, shown in Fig. 9 *c*, yields a value of $\tau_r = 200 \pm 5$ ns. A similar fit to the data in 75% glycerol-water (20°C) was obtained with $\tau_r = 685 \pm 50$ ns. (A comparison of a more extensive set of rotational correlation times with measurements from other techniques and with hydrodynamic theory is presented elsewhere (35)). The anisotropy decays at the individual degrees of photolysis (Fig. 9 *a* and *b*) were then fit using τ_r obtained from the average anisotropy decay to obtain $r(x, 0^+)$, the values of the absorption anisotropy at times that are short compared to τ_r.

The experimental values of $r(x, 0^+)$ are shown in Fig. 10. To compare these results with the theoretical prediction for a circular absorber, we use the short pulse approximation for the excitation pulse. This approximation is justified since the rotational correlation time of Mb under the present experimental conditions is long compared to the 10 ns pulse-width. In addition we observed no significant change in the amplitude of ligand rebinding as a function of the fraction photolyzed in the isotropically averaged data (Fig. 8), implying that there is little or no rebinding during the pulse. In water, comparison of the nanosecond geminate yield and absolute quantum yield measurements indicated that there was less than 1% subnanosecond geminate rebinding (29), and no subnanosecond geminate rebinding was detected in a picosecond study (36).

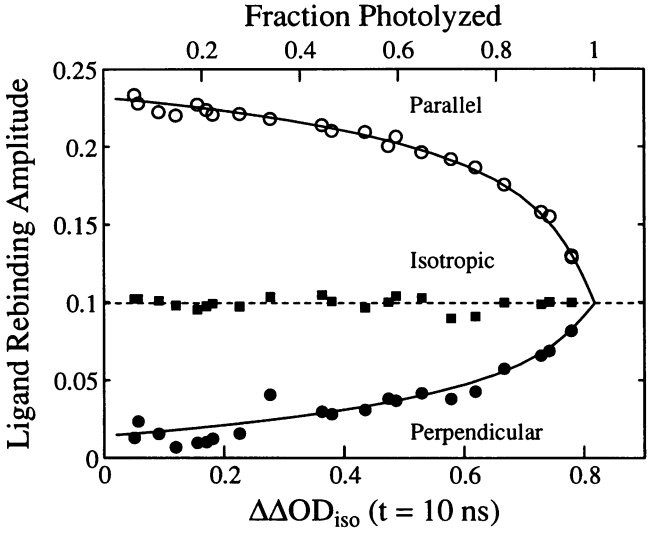

FIGURE 8 Effect of photoselection and rotational diffusion on the apparent ligand rebinding amplitudes. The fraction of photodissociated ligands that apparently rebind in the time interval 10 ns to 10 μs in 50% glycerol-water is plotted as a function of the amplitude of the isotropic difference spectrum $\Delta\Delta OD_{iso}$ (10 ns). The rebinding amplitudes, obtained using $1 - \Delta\Delta OD_{\|,\perp}$ (10 μs)/$\Delta\Delta OD_{\|,\perp}$ (10 ns), are plotted for measurements in which the polarization of the probe pulse was parallel (*open circles*) and perpendicular (*filled circles*) to the polarization of the excitation pulse. The isotropic amplitudes (*filled squares*) are also shown and the mean value ($\approx\Phi$ (10 μs)) is indicated by the dashed line. The fraction of hemes photolyzed, indicated on the top, is obtained using Eq. 25 with $\Delta\Delta OD_{max}$ (t = 10 ns) = 0.818. The solid lines through the polarized data are predicted values of the apparent ligand rebinding amplitudes, given by $1 - f_{\|,\perp}$ (10 μs)/$f_{\|,\perp}$ (10 ns), and are obtained using Eqs. 19 and 20 with $\langle P_2(\hat{n}(10\text{ ns})\cdot\hat{n}(0))\rangle \approx 1$, $\langle P_2(\hat{n}(10\ \mu s)\cdot\hat{n}(0))\rangle \approx 0$, and Φ (10 ns) ≈ 0. a_0 and a_2 are obtained using Eq. 33 for various values of the excitation intensity with $S = 0.95$; the corresponding values of the fraction photolyzed are given by $1 - a_0$.

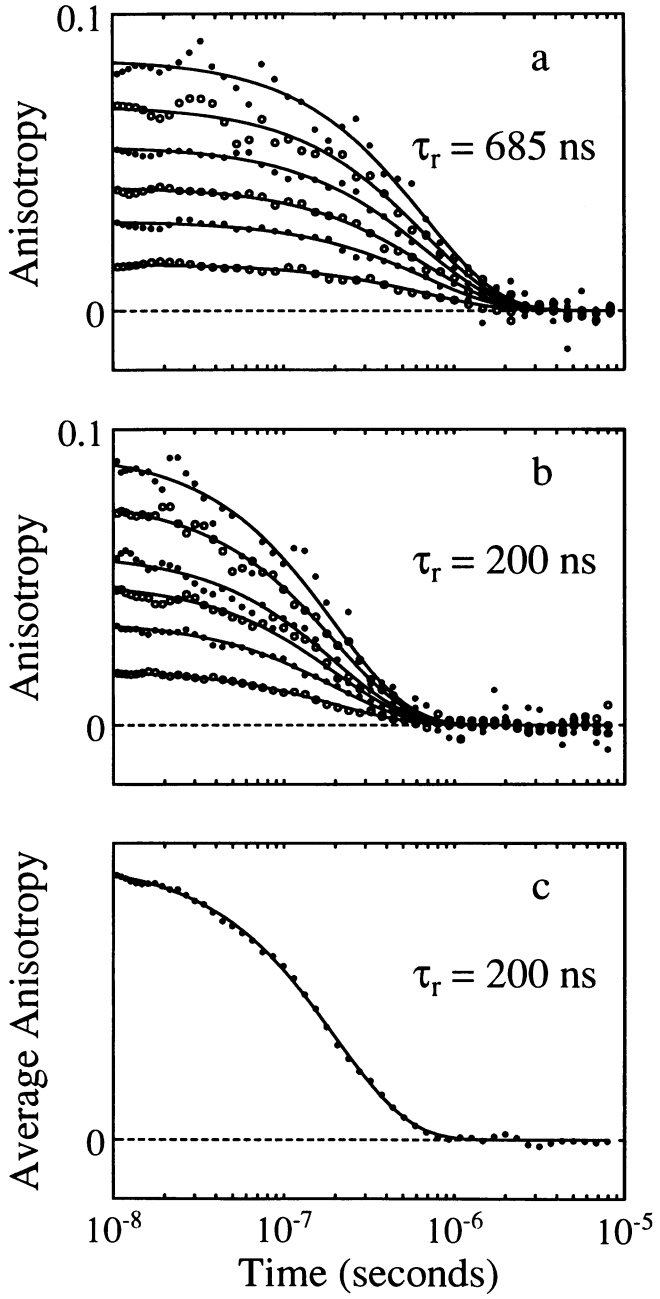

FIGURE 9 Photolysis dependence of the absorption anisotropy decay. (*a*, *b*) The absorption anisotropy decay $r(x, t)$, calculated using Eq. 21 is plotted as a function of time in (*a*) 75% glycerol-water at 20°C and at photolysis levels: 14, 52, 74, 83, 89, and 95%, and (*b*) 50% glycerol-water at 5°C and at photolysis levels: 6, 44, 76, 82, 91, and 95%. The continuous curves were obtained by fitting the data with an exponential curve with a time constant τ_r = 685 ns in *a* and τ_r = 200 ns in *b*. (*c*) The average anisotropy decay, obtained from a singular value decomposition of the decay curves in *b*, is plotted as a function of time. Prior to the SVD, the individual curves in *b* were weighted by the reciprocal of the noise in the curve. The continuous curve is an exponential fit to the data yielding a value of τ_r = 200 ± 5 ns, which is then used to fit the individual decay curves in *b*. Corresponding analysis of the data in *a* (not shown) yielded a value of τ_r = 685 ± 50 ns.

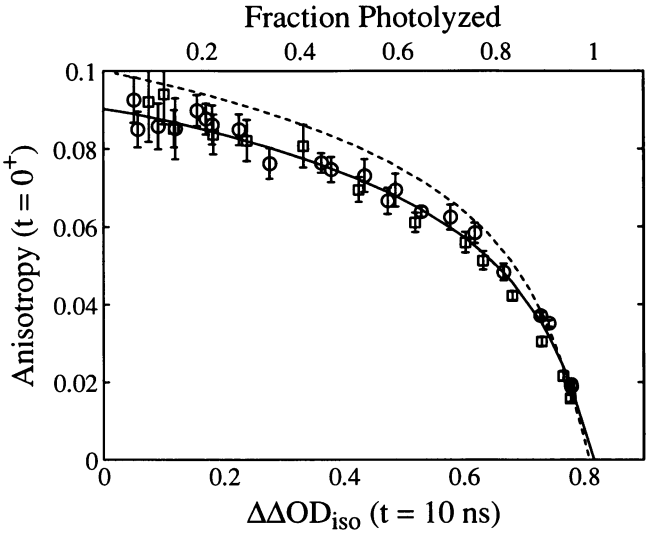

FIGURE 10 Photolysis dependence of the initial absorption anisotropy. The initial absorption anisotropy, $r(t = 0^+)$, obtained from an exponential fit to the anisotropy decay data in Fig. 9, is plotted as a function of the amplitude of the isotropic difference spectrum $\Delta\Delta OD_{iso}$ (t = 10 ns). Note that $t = 0^+$ refers to a time that is short enough that no overall reorientational motion of the molecule has occurred but long compared to the time-scales of internal motions. *Circles:* $r(t = 0^+)$ in 50% glycerol-water at 5°C; *squares:* $r(t = 0^+)$ in 75% glycerol-water at 20°C. The continuous curve is a fit to the data using the theory of a circular absorber undergoing rapid internal motions, as described in the text. The initial anisotropy, $r(t = 0^+)$, was calculated using Eq. 24, where a_0 and a_2 were calculated from Eq. 33. The fit yielded a value of 0.95 ± 0.02 for the order parameter S and 0.818 ± 0.01 for $\Delta\Delta OD_{max}$, the amplitude of the difference spectrum at infinite excitation intensity ($r(t = 0^+) = 0$). The fractional photolysis in the sample, given by $\Delta\Delta OD_{iso}/\Delta\Delta OD_{max}$, is indicated on the top axis. The dashed line is a fit to the data using the theory of a circular absorber that is rigidly attached to the protein molecule (S = 1).

From Eq. 23 the initial anisotropy is:

$$r(x, t = 0^+) = \frac{1}{10}\frac{a_2}{1 - a_0} \tag{24}$$

where $a_0 = (1 - x)$ and a_2 are given by Eqs. 12 and 15. The fraction of hemes photolyzed in each experiment is obtained from the amplitudes of the isotropic spectra:

$$x = 1 - a_0 = \frac{\Delta\Delta OD_{iso}\ (t = 10\text{ ns})}{\Delta\Delta OD_{max}\ (t = 10\text{ ns})} \tag{25}$$

where $\Delta\Delta OD_{max}$ is the amplitude at infinite laser power, when all the hemes are photolyzed. Since we do not have an accurate measure of the excitation intensity in each experiment we take the following approach to fitting the data. First a table of a_0 and a_2 are obtained from Eqs. 12 and 15, respectively, for various values of the excitation intensity. $\Delta\Delta OD_{max}$ is chosen as a single parameter to be varied in a least squares fit to the anisotropy measurements; varying the value of $\Delta\Delta OD_{max}$ changes the absolute fraction photolyzed (x) in each experiment. For each value of the parameter $\Delta\Delta OD_{max}$, a value of a_0 is obtained from Eq. 25 and the corresponding value of a_2

is obtained by interpolating on the tabulated values. The theoretical value of the initial anisotropy $r(x, 0^+)$ is then calculated using Eq. 24. The resulting least squares fit to the data is shown as the dashed line in Fig. 10. There are significant and systematic differences between the data and the fit: the experimental values at nearly all levels of photolysis are ~10% smaller than the theoretically predicted values. Several effects could potentially reduce the anisotropy relative to that calculated for a rigidly attached, circular absorber. These include deviations from perfectly circular absorption at either the excitation or probe wavelengths, a small tilt in the average orientation of the heme plane upon photodissociation, and rapid (sub-10 ns) equilibrium fluctuations of the heme orientation. In the following we discuss each of these effects, and conclude that fluctuations in the heme orientation make the biggest contribution to reducing the anisotropy.

Origins of reduced anisotropy

Deviations from circular absorption. Up to now we have treated the heme chromophore as a perfectly circular absorber of linearly polarized light. Circular absorption is a consequence of the fourfold symmetry of the heme. This symmetry requires that electric-dipole allowed transitions be either x,y-, or z-polarized, corresponding to a circular or linear absorber, respectively. The Soret and visible absorption bands arise from porphyrin $\pi \rightarrow \pi^*$ transitions, which are x,y-polarized and dominate the absorption in the wavelength range of our optical experiments (21). The data in Table 1 show that there is reasonably good agreement between the polarization ratios measured in the Soret region for single crystals of Mb, Hb, MbCO, and HbCO and those predicted for a circular absorber from the heme orientations in the crystal determined by x-ray crystallography (21, 37–47). The polarization ratio at the excitation wavelength for HbCO (532 nm) is also very close to that obtained from the areas of the Soret bands (Table 1), suggesting circular absorption at this wavelength as well.

The agreement of the predicted and measured polarization ratios is not exact, however, suggesting deviations from perfectly circular absorption. This is not surprising, since the fourfold symmetry must be reduced to some extent by the asymmetric perturbations of the axial ligands and the surrounding protein. The reduction in symmetry removes the two-fold degeneracy, separating the x and y components, which produces wavelength-dependent variations in the polarization ratios (21, 48, 49). It also mixes the porphyrin $\pi \rightarrow \pi^*$ transitions with other transitions of the heme or with transitions of the peptide backbone and amino acid side chains. The result of this mixing could introduce some ellipticity, i.e., one in which there is an imbalance of x- and y-polarized intensity, and one in which the plane of the absorption ellipse (the "optical" plane) may not correspond precisely to the plane of the porphyrin (the "geometric" plane). These effects could, in principle, account for some of the difference between the observed polarization ratios in single crystal spectra and those predicted from the orientation of the porphyrin plane determined by x-ray crystallography (Table 1).

In the preceding paper it is shown that, if the absorption at either the excitation or probe wavelengths is perfectly circular and the transition moment at the complementary wavelength has no z component, the limiting value ($t \rightarrow 0$, $I_0 \rightarrow 0$) for the absorption anisotropy is 0.1. It is also shown that elliptical absorption at both the excitation and probe wavelengths increases the value of the absorption anisotropy compared to that of a circular absorber. The only deviation from circular absorption that can reduce the absorption anisotropy is the presence of an underlying out-of-plane (i.e., z-) polarized transition at either wavelength. Such transitions can arise from iron-ligand charge transfer transitions or from iron $d \rightarrow d$ transitions (21, 50). A z-polarized component at the excitation wavelength increases the probability of photolyzing heme-CO complexes with their planes oriented perpendicular to the excitation polarization direction, and therefore reduces the anisotropy. Similarly, a z-polarized component at the probe wavelengths would lower the anisotropy. There is, of course, no anisotropy if the absorption at either the excitation or probe wavelengths is isotropic (i.e., spherically symmetric).

We now examine in more detail the effects of a z-polarized component at the excitation or probe wavelength on the anisotropy. From Eqs. 3.5, 3.8, and 3.24 of the preceding paper we obtain:

$$r(t) = \frac{1}{10}\frac{a_2}{1-a_0}\left[1 - \frac{\epsilon_B^0(\lambda_p)\beta_\parallel(\lambda_p) - \epsilon_A^0(\lambda_p)\alpha_\parallel(\lambda_p)}{\epsilon_B^0(\lambda_p) - \epsilon_A^0(\lambda_p)}\right] \times \langle P_2(\hat{\mathbf{n}}(t)\cdot\hat{\mathbf{n}}(0))\rangle, \quad (26)$$

where $\alpha_\parallel(\lambda_p)/3$ and $\beta_\parallel(\lambda_p)/3$ are the z-polarized fractions of the isotropic extinction coefficients at the probe wavelength, λ_p, in MbCO and Mb, respectively. We have used the relations $\sigma_A = 1 - \alpha_\parallel$ and $\sigma_B = 1 - \beta_\parallel$. a_0 and a_2 are given by Eqs. 3.17 and 3.18, respectively, of the preceding paper. In the limit of low excitation intensities, ($I_0 \rightarrow 0$), $a_0 \rightarrow 1 - \epsilon_A^0(\lambda_e)I_0$ and $a_2 \rightarrow (1 - \alpha_\parallel(\lambda_e))\epsilon_A^0(\lambda_e)I_0$. Substituting for a_0 and a_2 in Eq. 26, the anisotropy decay in the limit of low excitation intensities becomes:

$$r(t, I_0 \rightarrow 0) = \frac{1}{10}(1 - \alpha_\parallel(\lambda_e)) \times \left[1 - \frac{\epsilon_B^0(\lambda_p)\beta_\parallel(\lambda_p) - \epsilon_A^0(\lambda_p)\alpha_\parallel(\lambda_p)}{\epsilon_B^0(\lambda_p) - \epsilon_A^0(\lambda_p)}\right] \times \langle P_2(\hat{\mathbf{n}}(t)\cdot\hat{\mathbf{n}}(0))\rangle. \quad (27)$$

The results in Eqs. 26 and 27 show that when $\alpha_\parallel(\lambda_p) \neq \beta_\parallel(\lambda_p)$ the absorption anisotropy depends upon λ_p and that it diverges at wavelengths where $\epsilon_A^0(\lambda_p) = \epsilon_B^0(\lambda_p)$. If $\alpha_\parallel(\lambda_e) = 0$ and $\langle P_2(\hat{\mathbf{n}}(t)\cdot\hat{\mathbf{n}}(0)\rangle = 1$, the anisotropy at the wavelengths where $\epsilon_A^0 \gg \epsilon_B^0$ differs from the anisot-

TABLE 1 **Comparison of observed and predicted polarization ratios for crystals of Mb, Hb, MbCO, and HbCO**

Molecule	Observed		Predicted from heme orientation[b]			Reference
	Probe wavelengths (Soret band)[a]	Excitation wavelength (532 nm)	Circular absorber $\alpha_{\|\|} = 0$	Ellipsoidal absorber $\alpha_{\|\|} = 0.05$, $\alpha_{\|\|} = 0.10$		
Mb	1.3[c]	—	1.2	1.2	1.1	d
Mb	10.4[e]	—	11.9	8.6	6.7	f
Hb (*T*)	3.9[g]	—	4.3	3.9	3.5	h
Hb (*T*)	1.7[i]	—	1.7	1.7	1.6	j
Hb (*R*)	3.0[k]	—	3.1	3.0	2.7	l
MbCO	[m]	9.4[n]	10.3	7.8	6.2	o
HbCO (*R*)	2.1[p]	2.2[q]	2.6	2.4	2.3	r

[a]Calculated from the integrated area of the Soret bands in the two polarizations. The experimental uncertainties are all less than 2% (21). [b]For the circular absorber the polarization ratio was calculated from $\Sigma_i \sin^2 z_i\mu / \Sigma \sin^2 z_i\nu$ for the ellipsoidal absorber from $[(1 - (\alpha_{\|}/3))/2 \Sigma_i \sin^2 z_i\mu + \alpha_{\|}/3 \Sigma_i \cos^2 z_i\mu]/[(1 - (\alpha_{\|}/3))/2 \Sigma_i \sin^2 z_i\nu + \alpha_{\|}/3 \Sigma_i \cos^2 z_i\nu]$ (21, 37). In these expressions $z_i\mu$ and $z_i\nu$ are the angles between the heme normals, taken as the z molecular direction, and the crystal axes μ and ν, and $\alpha_{\|}/3$ is the fraction of the isotropic extinction coefficient due to the z-polarized transition, which is zero for the circular absorber, and has been calculated for $\alpha_{\|} = 0.05$ and $\alpha_{\|} = 0.10$ for the ellipsoidal absorber. The summation runs over the i hemes of the unit cell that are not related by a rotational or translational operation of the space group. The heme normals were calculated from the atomic coordinates as the normal to the least-squares best plane through the 24 porphin skeleton atoms. [c]From Eaton and Hofrichter (21). [d]Protein data bank file 2MBN (space group $P2_1$) (38). The coordinates were converted from an *abc** to an *a*bc* crystal axis system by a 16° rotation about the *b* axis. [e]From Eaton and Hofrichter (21); Makinen and Churg (39). [f]The structure of this crystal (space group $P2_12_12_1$) is only known for metMb (B. Katz, N. H. Xuong, W. Hendrickson, D. Lambright, and S. G. Boxer, unpublished results). To obtain a heme orientation for deoxyMb in this crystal, the backbone atoms from the x-ray structure for deoxyMb in the $P2_1$ space group were superposed onto the backbone atoms of the $P2_12_12_1$ metMb. The observed polarization ratio for the Soret band of this crystal was 8.8 (21, 39), while the predicted polarization ratio for a circular absorber is 13.5, and for an ellipsoidal absorber the polarization ratios are 9.4 ($\beta_{\|} = 0.05$) and 7.2 ($\beta_{\|} = 0.10$). [g]From Hofrichter et al. (40) for human deoxyhemoglobin in the *T* quaternary structure (high salt $P2_1$ space group). [h]From 0.17 nm coordinates of Fermi et al. (41) (Brookhaven Data Bank File 4HHB). The polarization ratio measurements were made with light incident on the (010) crystal face, which contains no crystal symmetry axis in this space group ($P2_1$). The axes of the polarization ratio measurements were therefore assumed to correspond to the axes of maximum and minimum absorption of the projection of the 4 hemes. The axis of maximum absorption was found to be at an angle of 2 degrees from the *c* crystal axis. [i]From Rivetti et al. (42) for deoxyhemoglobin in *T* quaternary structure (PEG $P2_1$ space group). [j]R. C. Liddington, unpublished results. [k]From Makinen and Eaton (43) for horse deoxyhemoglobin in *R* quaternary structure; see also Eaton and Hofrichter (21). [l]B. Luisi, unpublished results. [m]Sufficiently thin crystals to make polarization ratio measurements of the Soret band were not obtained in the study of Makinen and Churg (39). [n]From Makinen and Churg (39). [o]The structure of this crystal (space group $P2_12_12_1$) is only known for metMb (B. Katz, N. H. Xuong, W. Hendrickson, D. Lambright, and S. G. Boxer, unpublished results). To obtain a heme orientation for MbCO in this crystal, the backbone atoms from the x-ray structure for MbCO in $P2_1$ space group (44) were superposed onto the backbone atoms of the $P2_12_12_1$ metMb. See footnote f. [p]From Makinen and Eaton (43) for horse HbCO in *R* quaternary structure; see also Eaton and Hofrichter (21). [q]From Makinen and Eaton (45). [r]The structure of horse HbCO is not known. The heme orientation was calculated from the structure of human HbCO (46) after superposing backbone atoms onto the horse methemoglobin structure (Brookhaven Data Bank File 2MHB) (47).

ropy at the wavelengths where $\epsilon_B^0 \gg \epsilon_A^0$ by an amount that is approximately $0.1(\alpha_{\|} - \beta_{\|})$. Previously we obtained the anisotropy from the first SVD component of the transient spectra in the parallel and perpendicular geometries and ignored any wavelength dependent effects on the experimentally observed anisotropy. To explore the possibility of wavelength dependence we reconstructed the spectra at each degree of photolysis and polarization direction from the first 11 components of the SVD and recomputed the anisotropy at each wavelength and degree of photolysis using Eq. 2. In Fig. 11 we compare the initial anisotropy averaged over the wavelength region 413–429 nm for which $\epsilon_A^0(\lambda_p) > \epsilon_B^0(\lambda_p)$ with the corresponding values averaged over the wavelength region 431–449 nm for which $\epsilon_A^0(\lambda_p) < \epsilon_B^0(\lambda_p)$. The values are the same to within experimental errors at all degrees of photolysis. The theoretically predicted values for the initial anisotropy, averaged over the same two wavelength regions, for $\alpha_{\|} = 0.1$ and $\beta_{\|} = 0$, are also shown in Fig. 11. These results indicate that $\alpha_{\|}(\lambda_p)$ and $\beta_{\|}(\lambda_p)$ must differ by less than ~0.02.

An upper limit on the magnitude of an out-of-plane component that could account for the reduced anisotropy may be obtained by assuming that $\alpha_{\|}(\lambda_p) = \beta_{\|}(\lambda_p) = 0$ and that all the reduction comes from $\alpha_{\|}(\lambda_e)$, the out-of-plane component at the excitation wavelength. A least-squares fit to the anisotropy data in Fig. 10, using Eq. 26 and calculating a_0 and a_2 as a function of the parameter $\alpha_{\|}(\lambda_e)$ in Eqs. 3.17 and 3.18 of the preceding paper (using $\sigma_A = 1 - \alpha_{\|}$), yields a value of $\alpha_{\|}(532\ \text{nm}) = 0.1 \pm 0.05$, which is equivalent to 3% of the isotropic extinction coefficient. Similarly, if it is assumed that $\alpha_{\|}(\lambda_p) = \beta_{\|}(\lambda_p)$ and $\alpha_{\|}(\lambda_e) = 0$, then an upper limit of 0.1 is found for $\alpha_{\|}(\lambda_p)$ $(=\beta_{\|}(\lambda_p))$. If the out-of-plane component is present at both excitation and probe wavelengths, then the contribution at these wavelengths could, of course, be less than 3%. For example, the anisotropy data can be fit with $\beta_{\|}(\lambda_p) = \alpha_{\|}(\lambda_p) = \alpha_{\|}(\lambda_e) = 0.05$, corresponding to 1.7% of the isotropic extinction coefficient.

Additional information on the magnitude of z-polarized components is available from polarized absorption

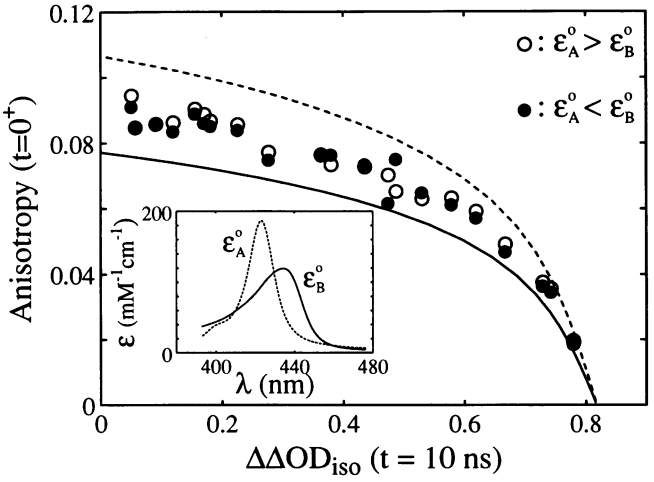

FIGURE 11 Wavelength dependence of the initial absorption anisotropy. The initial absorption anisotropy averaged over the wavelength region 413–429 nm for which $\epsilon_A^0 > \epsilon_B^0$ (*open circles*) is plotted versus the amplitude of the isotropic difference spectrum at 10 ns, along with the initial anisotropy averaged over the wavelength region 431–449 nm for which $\epsilon_A^0 < \epsilon_B^0$ (*filled circles*). In order to obtain the average anisotropy in the two wavelength regions, the wavelength-dependent anisotropy, $r(x, t, \lambda_p)$, calculated from Eq. 2 for the data in 50% glycerol at 5°C, was fit with an exponential having a time constant 200 ns; the amplitudes from the exponential fits yielded $r(x, 0^+, \lambda_p)$. Since the noise in the anisotropy is large at the wavelengths where the optical density is small, the average anisotropy was calculated after weighting the anisotropy by the square of the first U component:

$$\bar{r}(x, 0^+) = \frac{\sum_{\lambda_p} r(x, 0^+, \lambda_p)[U_1(\lambda_p)]^2}{\sum_{\lambda_p} [U_1(\lambda_p)]^2}.$$

The lines are the initial average anisotropies calculated from Eq. 26 with $\alpha_\parallel(\lambda_p) = 0.1$ and $\beta_\parallel(\lambda_p) = 0$; a_0 $(=1 - x)$ and a_2 are calculated using Eqs. 12 and 15. The values of the extinction coefficients ϵ_A^0 and ϵ_B^0 used in Eq. 26 are shown in the inset. The dashed curve is the initial anisotropy averaged over the wavelength region 413–429 nm while the continuous curve is the average over the wavelength region 431–449 nm.

measurements on single crystals. Table 1 compares the observed polarization ratios and those predicted from the heme orientations in single crystals determined by x-ray crystallography. In each case the polarization ratio at the probe wavelengths is defined as the ratio of the integrated band area for the Soret band for light polarized parallel to two crystal directions. A *z*-polarized component always lowers the observed polarization ratio compared to that of a circular absorber. For the deoxyheme spectra (Mb and Hb in both quaternary structures), the data in Table 1 indicate that there is a small *z*-polarized component, with $\beta_\parallel(\lambda_p)$ closer to 0.05 than to 0.1.

It is difficult to reach any firm conclusions about the magnitude of the *z*-polarized component in the CO complex, since there are as yet no optical measurements on crystals for which the x-ray structure has been determined.[3] The polarized measurements on HbCO, however, indicate that the *z*-polarized component in the CO complex is the same at the excitation and probe wavelengths, i.e., $\alpha_\parallel(\lambda_e) \approx \alpha_\parallel(\lambda_p)$. The above observation, together with the lack of any wavelength dependence to the anisotropy measured in the Soret band, suggests that $\beta_\parallel(\lambda_p) \approx \alpha_\parallel(\lambda_p) \approx \alpha_\parallel(\lambda_e) \approx 0.05$.[4] Considering the difference in electronic structures of deoxy and carbonmonoxy hemes, it would be surprising if the fraction of *z*-polarized intensity from underlying charge transfer or $d \rightarrow d$ transitions were the same at all three wavelengths. We shall see below, however, that a *z*-polarized component resulting from an underlying *z*-polarized electronic transition cannot be distinguished from an apparent *z*-polarized component resulting from fluctuations in the orientation of the heme plane that are fast compared to the length of the optical pulse. Both the crystal polarization ratios and the solution anisotropy data could be consistently explained if there were no contribution from *z*-polarized transitions and if the fluctuations in the orientation of carbonmonoxy- and deoxy hemes were very similar. This situation would give rise to apparent *z*-polarized components with $\beta_\parallel(\lambda_p) \approx \alpha_\parallel(\lambda_p) \approx \alpha_\parallel(\lambda_e) \approx 0.05$.

A tilt in the heme plane. The absorption anisotropy would be reduced by a subnanosecond change in the orientation of the heme plane. Comparison of the x-ray structures of MbCO and Mb shows that the angle between the heme normals is 3.5°. If the normal to the heme plane in Mb tilts by an angle γ relative to its orientation in MbCO, then from Eq. 3.23 of the preceding paper we obtain:

$$r(t = 0^+) = \frac{1}{10}\frac{a_2}{1 - a_0}\left[\frac{\epsilon_B(\lambda_p)P_2(\cos\gamma) - \epsilon_A(\lambda_p)}{\epsilon_B(\lambda_p) - \epsilon_A(\lambda_p)}\right] \quad (28)$$

and, in the limit of low excitation intensities and for small values of γ, we have

$$r(t = 0^+, I_0 \rightarrow 0, \gamma \rightarrow 0) = \frac{1}{10}\left[1 - \frac{3}{2}\gamma^2\frac{\epsilon_B^0}{\epsilon_B^0 - \epsilon_A^0}\right]. \quad (29)$$

As is the case for an out-of-plane component, a tilt in the plane of absorption upon excitation introduces wavelength-dependent effects. It is interesting to note that when $\epsilon_A^0(\lambda_p) > \epsilon_B^0(\lambda_p)$ the absorption anisotropy from

[3] For HbCO the optical measurements were made on horse hemoglobin crystals (space group C2), while the x-ray data is only available for human HbCO for a crystal in a different space group ($P2_1$). In the case of MbCO, the optical measurements were made on metMb (space group $P2_12_12_1$), while the x-ray data is available for MbCO in the space group $P2_1$.

[4] The lower polarization ratio of 2.1–2.2 in HbCO compared to the predicted value of 2.4 for $\alpha_\parallel = 0.05$ could arise from a small difference in the orientation of the heme plane in horse HbCO compared to human HbCO. A difference of as little as 2° could account for the difference in polarization ratios.

Eq. 29 is greater than that predicted for a circular absorber and when $\epsilon_A^0(\lambda_p) < \epsilon_B^0(\lambda_p)$, the absorption anisotropy is smaller. The largest deviations occur where the difference spectrum is small. The very small angle of the heme tilt observed in a comparison of the MbCO and Mb crystal structures ($\gamma = 3.5° = 0.06$ radians), together with the lack of any wavelength dependence observed in the experimental anisotropies suggests that the heme tilt does not contribute significantly to lowering the anisotropy. For instance, at the wavelengths where $\epsilon_B^0(\lambda_p) \gg \epsilon_A^0(\lambda_p)$, the anisotropy is predicted to be lowered by only 0.5%.

Rapid internal motion of the heme. Equilibrium fluctuations in the heme orientation that are not resolved by the 10 ns pulses used in our experiments could also lower the anisotropy. Under the present experimental conditions the overall diffusive motion of the molecule is slow. Internal motions that produce changes in the orientation of the heme plane could, however, occur on a time-scale that is short compared to the pulse-width. For a δ-function excitation pulse the change in optical density and anisotropy are still given by Eqs. 14 and 22, but in evaluating the reorientational correlation function these internal motions must be taken into account. We assume, for the sake of simplicity, that the normal to the heme plane can fluctuate ("wobble") in an axially symmetric way about some axis fixed in the molecule. If the internal motions are fast and independent of the diffusive motions of the entire molecule, Lipari and Szabo (51) showed that, for a δ-function excitation pulse and at times long compared to the time-scale of internal motions, the correlation function becomes $S^2 \exp(-t/\tau_r)$. The order parameter S ($0 \le S \le 1$) is defined in Eq. 3.31 of the preceding paper. If the internal motions of the heme are modelled as the normal to the heme plane wobbling in a cone of semiangle θ_0, then:

$$S = \tfrac{1}{2} \cos\theta_0 (1 + \cos\theta_0). \tag{30}$$

The general situation when the internal motions and the overall diffusive motion of the macromolecule occur within the excitation pulse is formally described in the previous paper. If the excitation pulse is long enough, so that the system reaches equilibrium with respect to the fast internal motions, the absorber behaves as if it has an effective out-of-plane component. Assuming that the fluctuations are the same in the two states of the system, the apparent out-of-plane components are related to the order parameter by:

$$\alpha_\parallel = \beta_\parallel = 1 - S, \tag{31}$$

and the anisotropy decay from Eq. 26 becomes:

$$r(t) = \frac{S}{10} \frac{a_2}{1 - a_0} \exp(-t/\tau_r), \tag{32}$$

where the correlation function in Eq. 26 is an exponentially decaying function for a molecule that undergoes isotropic rotational diffusion; a_0 and a_2 are obtained from Eqs. 3.17 and 3.18 of the preceding paper with $\sigma = S$:

$$a_0 = \frac{1}{2} \int_0^\pi \exp[-\epsilon_A^0(\lambda_e) I_0 (1 - SP_2(\cos\theta))] \sin\theta \, d\theta$$

$$a_2 = \frac{5}{2} \int_0^\pi \exp[-\epsilon_A^0(\lambda_e) I_0 (1 - SP_2(\cos\theta))] \times P_2(\cos\theta) \sin\theta \, d\theta. \tag{33}$$

In the limit of low intensities ($I_0 \to 0$: $a_0 \to 1 - \epsilon_A^0(\lambda_e) I_0$ and $a_2 \to S\epsilon_A^0(\lambda_e) I_0$) we recover the result of Lipari and Szabo (51):

$$r(t, I_0 \to 0) = \frac{S^2}{10} \exp(-t/\tau_r). \tag{34}$$

A least-squares fit to the anisotropy data in Fig. 10 using Eqs. 32 and 33, yields a value of $S = 0.95 \pm 0.02$. From Eq. 30 this value of S corresponds to a cone of semiangle $\theta_0 = 14.9° \pm 2.6°$. As pointed out above, an effective out-of-plane component ($1 - S = 0.05$) at both excitation and probe wavelengths is consistent with the polarization ratios obtained from the crystals (Table 1). Since the polarization measurements on the crystals are not time-resolved they do not distinguish between any real out-of-plane component and contributions from internal motions of the heme. The fit also yields a value of $\Delta\Delta OD_{max}$ ($t = 10$ ns) $= 0.82 \pm 0.01$. $\Delta\Delta OD_{max}$ is the amplitude of the difference spectrum at 100% photolysis and corresponds to the amplitude at which the anisotropy extrapolates to zero. The degree of photolysis is therefore obtained, using Eq. 25, to an accuracy of $\sim 1\%$.

An accurate assessment of the relative contributions of internal motion and z-polarized transitions to the decrease in the apparent order parameter in myoglobin will require time resolution of the decay in the anisotropy. Experiments along these lines have already been performed for hemoglobin by Hochstrasser and co-workers (25). In their experiments the anisotropy in the CO infrared absorption after partial photolysis was found to be constant between 30 fs and 1 ns. Their data, however, were not sufficiently accurate to detect an anisotropy decay of the magnitude observed in myoglobin.

A theoretical estimate of the contribution of the internal dynamics of the heme to decreasing the apparent order parameter is made from molecular dynamics simulations in the accompanying paper by Henry (28). In principle one should evaluate the time dependence of both reorientational correlation functions of Eq. 13, i.e., $\langle P_2(\hat{\mathbf{n}}_B(t) \cdot \hat{\mathbf{n}}_A(0)) \rangle$ and $\langle P_2(\hat{\mathbf{n}}_A(t) \cdot \hat{\mathbf{n}}_A(0)) \rangle$. Only the second correlation function can be evaluated with current simulation capabilities, since evaluation of the first requires a separate trajectory that simulates photolysis for each time point. If one assumes that the internal dynamics of the heme are unaffected by photodissociation (apart from the heme tilt which we have shown has a negligible effect in reducing the anisotropy), then the

reorientational correlation function can be evaluated from a single trajectory for either Mb or MbCO. From a 2 ns trajectory of MbCO Henry has found that the reorientational correlation function shows a very rapid (subpicosecond) decay to a value of about 0.99 ($=S^2$), and decays further via what appears to be a single global conformational transition to a value of ~0.97, corresponding to $S = 0.985$. Since the 2 ns trajectory can only explore a small part of conformational space, 0.985 must be considered as an upper limit. Thus, internal motion of the heme plane is theoretically predicted to account for at least 30% of the decrease in the apparent order parameter.

CONCLUSIONS

As predicted by the theoretical analysis, the experimental results presented here show that photoselection produces large deviations from the true geminate ligand rebinding curves for myoglobin. These deviations are substantial even when the degree of photolysis is greater than 90%. The effects of photoselection and rotational diffusion are completely eliminated by calculating the isotropically averaged optical densities from measurements in which the polarization of the probe pulse is both parallel and perpendicular to that of the excitation pulse.

The experiments also yield the optical anisotropy prior to rotational diffusion, which is lower than the value for a rigidly attached heme chromophore exhibiting perfectly circular absorption. The decrease can be expressed in terms of an apparent order parameter, S, which has a value of 0.95 ± 0.02. The change in the average orientation of the heme plane observed in the crystals of Mb and MbCO has a negligible effect on lowering the apparent order parameter from the ideal value of 1.00. The two remaining possibilities are the presence of an underlying z-polarized transition, and internal motion of the heme that is fast compared to the 10 ns optical pulses of our experiments. Polarized single crystal data suggest that most of the decreased anisotropy arises from fluctuations in the heme orientation. This conclusion is supported by steady state fluorescence experiments on myoglobin from which the iron has been removed (52). The contribution from heme dynamics is discussed further in the accompanying paper by Henry (28), which suggests that at least 30% of the decrease in the apparent order parameter results from internal motion of the heme.

The relative contributions of z-polarized transitions and heme motion can, in principle, be distinguished by determining the initial anisotropy using much shorter laser pulses, and time resolving the decay in the anisotropy that occurs prior to rotational diffusion of the entire molecule. This becomes a particularly attractive experiment since the simulation data suggest that internal motion of the heme arises largely from transitions between conformational substates associated with global motions of the protein atoms (28). Time resolution of the anisotropy decay should therefore provide information on the dynamics of interconversion of myoglobin conformational substates.

We are very much indebted to Attila Szabo for his continuous help throughout the course of this work. We also thank Steven Boxer, Robert Liddington, and Ben Luisi for providing us with unpublished x-ray coordinates.

Received for publication 4 August and in final form 15 October 1992.

REFERENCES

1. Austin, R. H., K. W. Beeson, L. Eisenstein, H. Frauenfelder, and I. C. Gunsalus. 1975. Dynamics of ligand binding to myoglobin. *Biochemistry.* 14:5355–5373.
2. Beece, D., L. Eisenstein, H. Frauenfelder, D. Good, M. C. Marden, L. Reinisch, A. H. Reynolds, L. B. Sorensen, and K. T. Yue. 1980. Solvent viscosity and protein dynamics. *Biochemistry.* 19:5147–5157.
3. Sawicki, C. A., and Q. H. Gibson. 1976. Quaternary conformational change in human hemoglobin studied by laser photolysis or carboxyhemoglobin. *J. Biol. Chem.* 251:1533–1542.
4. Greene, B. I., R. M. Hochstrasser, R. B. Weisman, and W. A. Eaton. 1978. Spectroscopic studies of oxy- and carbonmonoxyhemoglobin after pulsed optical excitation. *Proc. Natl. Acad. Sci. USA.* 75:5255–5259.
5. Duddell, D. A., R. J. Morris, and J. T. Richards. 1979. Ultra-fast recombination in nanosecond laser photolysis of carbonylhaemoglobin. *J. C. S. Chem. Comm.* 75–76.
6. Chernoff, D. A., R. M. Hochstrasser, and A. W. Steele. 1980. Geminate recombination of O_2 and hemoglobin. *Proc. Natl. Acad. Sci. USA.* 77:5605–5610.
7. Martin, J. L., A. Migus, C. Poyart, Y. Lecarpentier, R. Astier, and A. Antonetti. 1983. Femtosecond photolysis of CO-ligated protoheme and hemoproteins: appearance of deoxy species with a 350-fsec time constant. *Proc. Natl. Acad. Sci. USA.* 80:173–177.
8. Hofrichter, J., J. H. Sommer, E. R. Henry, and W. A. Eaton. 1983. Nanosecond absorption spectroscopy of hemoglobin: elementary processes in kinetic cooperativity. *Proc. Natl. Acad. Sci. USA.* 80:2235–2239.
9. Henry, E. R., M. Levitt, and W. A. Eaton. 1985. Molecular dynamics simulation of photodissociation of carbon monoxide from hemoglobin. *Proc. Natl. Acad. Sci. USA.* 82:2034–2038.
10. Friedman, J. 1985. Structure, dynamics, and reactivity in hemoglobin. *Science (Wash. DC).* 228:1273–1280.
11. Murray, L. P., J. Hofrichter, E. R. Henry, M. Ikeda-Saito, K. Kitagishi, T. Yonetani, and W. A. Eaton. 1988. The effect of quaternary structure on the kinetics of conformational changes and nanosecond geminate rebinding of carbon monoxide to hemoglobin. *Proc. Natl. Acad. Sci. USA.* 85:2151–2155.
12. Anfinrud, P. A., C. Han, and R. M. Hochstrasser. 1989. Direct observations of ligand dynamics in hemoglobin by subpicosecond infrared spectroscopy. *Proc. Natl. Acad. Sci. USA.* 86:8387–8391.
13. Steinbach, P. J., A. Ansari, J. Berendzen, D. Braunstein, K. Chu, B. R. Cowen, D. Ehrenstein, H. Frauenfelder, J. B. Johnson, D. C. Lamb, S. Luck, J. R. Mourant, G. U. Nienhaus, P. Ormos, R. Philipp, A. Xie, R. D. Young. 1991. Ligand binding to heme proteins: connection between dynamics and function. *Biochemistry.* 30:3988–4001.
14. Eaton, W. A., E. R. Henry, and J. Hofrichter. 1991. Application of linear free energy relations to protein conformational changes:

The quaternary structural change of hemoglobin. *Proc. Natl. Acad. Sci. USA.* 88:4472–4475.

15. Lambright, D. G., S. Balasubramaniam, and S. G. Boxer. 1991. Protein relaxation dynamics in human myoglobin. *Chem. Phys.* 158:249–260.
16. Ansari, A., C. M. Jones, E. R. Henry, J. Hofrichter, and W. A. Eaton. 1992. The role of solvent viscosity in the dynamics of protein conformational changes. *Science (Wash. DC).* 256:1796–1798.
17. Marden, M. C., E. S. Hazard, and Q. H. Gibson. 1986. Testing the two-state model: anomalous effector binding to human hemoglobin. *Biochemistry.* 25:7591–7596.
18. Hofrichter, J., E. R. Henry, A. Szabo, L. P. Murray, A. Ansari, C. M. Jones, M. Coletta, M. Falcioni, M. Brunori, and W. A. Eaton. 1991. Dynamics of the quaternary conformational change in trout hemoglobin. *Biochemistry.* 30:6583–6598.
19. Jones, C. M., A. Ansari, E. R. Henry, G. W. Christoph, J. Hofrichter, and W. A. Eaton. 1992. Speed of intersubunit communication in proteins. *Biochemistry.* 31:6692–6702.
20. Albrecht, A. C. 1961. Polarizations and assignments of transitions: the method of photoselection. *J. Mol. Spectr.* 6:84–108.
21. Eaton, W. A., and J. Hofrichter. 1981. Polarized absorption and linear dichroism spectroscopy of hemoglobin. *Meth. Enzymol.* 76:175–261.
22. Lewis, J. W., and D. S. Kliger. 1991. Rotational diffusion effects on absorbance measurements: limitations to the magic-angle approach. *Photochem. Photobiol.* 54:963–968.
23. Moore, J. N., P. A. Hansen, and R. M. Hochstrasser. 1987. A new method for picosecond time-resolved infrared spectroscopy: applications to CO photodissociation from iron porphyrins. *Chem. Phys. Lett.* 138:110–114.
24. Moore, J. N., P. A. Hansen, and R. M. Hochstrasser. 1988. Iron-carbonyl bond geometries of carboxymyoglobin and carboxyhemoglobin in solution determined by picosecond time-resolved infrared spectroscopy. *Proc. Natl. Acad. Sci. USA.* 85:5062–5066.
25. Locke, B., T. Lian, and R. M. Hochstrasser. 1991. Determination of Fe-CO geometry and heme rigidity in carbonmonoxyhemoglobin using femtosecond IR spectroscopy. *Chem. Phys.* 158:409–419.
26. Ormos, P., D. Braunstein, H. Frauenfelder, M. K. Hong, S-L. Lin, T. D. Sauke, and R. D. Young. 1988. Orientation of carbon monoxide and structure-function relationship in carbonmonoxymyoglobin. *Proc. Natl. Acad. Sci. USA.* 85:8492–8496.
27. Ansari, A., and A. Szabo. 1992. Theory of photoselection by intense light pulses: the influence of reorientational dynamics and chemical kinetics on absorbance measurements. *Biophys. J.* 64:838–851.
28. Henry, E. R. 1992. Molecular dynamics simulations of heme reorientational motions in myoglobin. *Biophys. J.* 64:869–885.
29. Henry, E. R., J. H. Sommer, J. Hofrichter, and W. A. Eaton. 1983. Geminate recombination of carbon monoxide to myoglobin. *J. Mol. Biol.* 166:443–451.
30. Hofrichter, J., E. R. Henry, J. H. Sommer, R. Deutsch, M. Ikeda-Saito, T. Yonetani, and W. A. Eaton. 1985. Nanosecond optical spectra of iron-cobalt hybrid hemoglobins: geminate recombination, conformational changes, and intersubunit communication. *Biochemistry.* 24:2667–2679.
31. Hofrichter, J., E. R. Henry, A. Ansari, C. M. Jones, R. M. Deutsch, and J. Sommer. 1992. Ligand binding and conformational changes measured by time-resolved absorption spectroscopy. *Meth. Enzymol.* 210:129–192.
32. Golub, G. H., and C. Reinsch. 1970. Singular value decomposition and least-squares solutions. *Numerische Mathematik.* 14:403–420.
33. Henry, E. R., and J. Hofrichter. 1992. Singular value decomposition: application to analysis of experimental data. *Meth. Enzymol.* 210:129–192.
34. Nagle, J. F., S. M. Bhattacharjee, L. A. Parodi, and R. H. Lozier. 1983. Effect of photoselection upon saturation and the dichroic ratio in flash experiments upon effectively immobilized systems. *Photochem. Photobiol.* 38:331–339.
35. Hofrichter, J., C. M. Jones, A. Ansari, E. R. Henry, O. Schaad, and W. A. Eaton. 1993. Rotational diffusion of myoglobin and hemoglobin. *Biophys. J.* 64:A271.
36. Janes, S. M., G. A. Dalickas, W. A. Eaton, and R. M. Hochstrasser. 1988. Picosecond transient absorption study of photodissociated carboxy hemoglobin and myoglobin. *Biophys. J.* 54:545–549.
37. Hofrichter, J., and W. A. Eaton. 1976. Linear dichroism of biological chromophores. *Annu. Rev. Biophys. Bioeng.* 5:511–560.
38. Takano, T. 1977. Structure of myoglobin refined at 2.0 Å resolution. *J. Mol. Biol.* 110:537–568.
39. Makinen, M. W., and A. K. Churg. 1983. Structural and analytical aspects of the electronic spectra of hemeproteins. *In* Iron Porphyrins, Part I. A. B. P. Lever and H. B. Gray, editors. Addison-Wesley Publishing Co., London. 141–235.
40. Hofrichter, J., D. G. Hendricker, and W. A. Eaton. 1973. Orientation of hemoglobin S fibers: optical determination of the molecular orientation in sickled erythrocytes. *Proc. Natl. Acad. Sci. USA.* 70:3604–3608.
41. Fermi, G., M. F. Perutz, B. Shaanan, and F. Fourme. 1984. The crystal structure of human deoxyhaemoglobin at 1.74 Å resolution. *J. Mol. Biol.* 175:159–174.
42. Rivetti, C., A. Mozzarelli, G. L. Rossi, E. R. Henry, and W. A. Eaton. 1993. Oxygen binding by single crystals of hemoglobin. *Biochemistry.* In press.
43. Makinen, M. W., and W. A. Eaton. 1974. Optically-detected conformational changes in hemoglobin single crystals. *Nature (Lond.).* 247:62–64.
44. Kuriyan, J., S. Wilz, M. Karplus, and G. A. Petsko. 1986. X-ray structure and refinement of carbon-monoxy (Fe-II)-myoglobin at 1.5 Å resolution. *J. Mol. Biol.* 192:133–154.
45. Makinen, M. W., and W. A. Eaton. 1973. Polarized single crystal absorption spectra of carboxy- and oxyhemoglobin. *Ann. NY Acad. Sci.* 206:210–222.
46. Derewenda, Z., G. Dodson, P. Emsley, D. Harris, K. Nagai, M. F. Perutz, and J.-P. Reynaud. 1990. Stereochemistry of carbon monoxide binding to normal human adult and Cowtown haemoglobins. *J. Mol. Biol.* 211:515–519.
47. Ladner, R. C., E. G. Heidner, and M. F. Perutz. 1977. The structure of horse methaemoglobin at 2.0 angstroms resolution. *J. Mol. Biol.* 114:385–414.
48. Eaton, W. A., and R. M. Hochstrasser. 1967. Electronic spectrum of single crystals of ferricytochrome c. *J. Chem. Phys.* 46:2533–2543.
49. Eaton, W. A., and R. M. Hochstrasser. 1968. Single crystal spectra of ferrimyoglobin complexes in polarized light. *J. Chem. Phys.* 49:985–995.
50. Eaton, W. A., L. K. Hanson, P. J. Stephens, and J. C. Sutherland. 1978. Optical spectra of oxy- and deoxyhemoglobin. *J. Am. Chem. Soc.* 100:4991–5003.
51. Lipari, G., and A. Szabo. 1980. Effect of librational motion on fluorescence depolarization and nuclear magnetic resonance relaxation in macromolecules and membranes. *Biophys. J.* 30:489–506.
52. Royer, C. A., and B. Alpert. 1987. Porphyrin dynamics in the heme pockets of myoglobin and hemoglobin. *Chem. Phys. Lett.* 134:454–460.